Cerebral Cortex Advance Access published January 9, 2015

OXFORD

Cerebral Cortex, 2015, 1–19

doi: 10.1093/cercor/bhu301
Original Article

ORIGINAL ARTICLE

Fine Tuning of Synaptic Plasticity and Filtering by GABA Released from Hippocampal Autaptic Granule Cells

Pierluigi Valente[1,2], Marta Orlando[1], Andrea Raimondi[1], Fabio Benfenati[1,2], and Pietro Baldelli[1,2]

[1]Department of Neuroscience and Brain Technologies, Istituto Italiano di Tecnologia, Genova 16163, Italy, and [2]Department of Experimental Medicine, Section of Physiology, University of Genova, Genova 16132, Italy

Address correspondence to Pietro Baldelli, Department of Experimental Medicine, School of Medicine and Pharmacy, University of Genova, Viale Benedetto XV 3, Genova 16132, Italy. Email: pietro.baldelli@unige.it

Abstract

The functional consequence of γ-aminobutyric acid (GABA) release at mossy fiber terminals is still a debated topic. Here, we provide multiple evidence of GABA release in cultured autaptic hippocampal granule cells. In ~50% of the excitatory autaptic neurons, GABA, VGAT, or GAD67 colocalized with vesicular glutamate transporter 1-positive puncta, where both $GABA_B$ and $GABA_A$ receptors (Rs) were present. Patch-clamp recordings showed a clear enhancement of autaptic excitatory postsynaptic currents in response to the application of the $GABA_B$R antagonist CGP58845 only in neurons positive to the selective granule cell marker Prox1, and expressing low levels of GAD67. Indeed, GCP non-responsive excitatory autaptic neurons were both Prox1- and GAD67-negative. Although the amount of released GABA was not sufficient to activate functional postsynaptic $GABA_A$Rs, it effectively activated presynaptic $GABA_B$Rs that maintain a tonic "brake" on the probability of release and on the size of the readily releasable pool and contributed to resting potential hyperpolarization possibly through extrasynaptic $GABA_A$R activation. The autocrine inhibition exerted by $GABA_B$Rs on glutamate release enhanced both paired-pulse facilitation and post-tetanic potentiation. Such $GABA_B$R-mediated changes in short-term plasticity confer to immature granule cells the capability to modulate their filtering properties in an activity-dependent fashion, with remarkable consequences on the dynamic behavior of neural circuits.

Key words: $GABA_B$ receptors, GABA-glutamate corelease, granule cells, short-term plasticity, synaptic filtering

Introduction

The notion that neurons can release more than 1 transmitter, initially proposed by the pioneering work of Thomas Hökfelt (Hökfelt et al. 1980), is now widely accepted. Neuropeptides stored in large dense-core vesicles are frequently colocalized and coreleased by monoaminergic, cholinergic, and GABAergic neurons (see Hnasko and Edwards 2012 for review). However, for many years, it has generally been assumed that neurons could release only one of the classical neurotransmitters (NTs), such as glutamate or γ-aminobutyric acid (GABA), which mediate the vast majority of excitatory and inhibitory transmission in the brain. Thus, while glutamatergic and GABAergic synaptic vesicles (SVs) share H^+-ATPase (Forgac 2007), they express distinct vesicular NT transporters such as vesicular glutamate transporters (VGLUT) 1, 2, and 3 and vesicular GABA transporter (VGAT) (Edwards 2007; Grønborg et al. 2010).

In the last years, an increasing amount of experimental evidence has demonstrated an abundant coexpression of VGLUT1 and VGAT in retina bipolar cells as well as in cortical and hippocampal glutamatergic synapses (Kao et al. 2004; Fattorini et al. 2009; Zander et al. 2010). Moreover, electrophysiological studies suggested that GABA is coreleased from glutamatergic hippocampal mossy fiber terminals (MFTs) during postnatal development (Walker et al. 2001; Gutiérrez 2003; Safiulina et al. 2006) or

in the adult after induction of hyperexcitability (Gutiérrez 2000; Gutiérrez and Heinemann 2001; Gómez-Lira et al. 2002; Romo-Parra et al. 2003; Treviño and Gutiérrez 2005). Although initially argued (Uchigashima et al. 2007), the growing and convincing experimental evidence (Safiulina et al. 2006; for review, see Gutiérrez 2009; Beltrán and Gutiérrez 2012; Cabezas et al. 2012) strengthened considerably the notion of GABA corelease at MFs. Previous data have shown that GABA, coreleased at these glutamatergic synapses, mainly activates postsynaptic (Gutiérrez 2003; Safiulina et al. 2006) and presynaptic (Ruiz et al. 2003) ionotropic type A GABA receptors ($GABA_A$Rs). More recently, GABA release at immature MF–CA3 connections was shown not only to evoke inhibitory postsynaptic currents (IPSCs) but also to negatively modulate the probability of GABA release at MFTs (Safiulina and Cherubini 2009) via the activation of presynaptic G-protein-coupled type B GABA receptors ($GABA_B$Rs). Interestingly, presynaptic $GABA_B$ autoreceptors activated by GABA released from granule cells (GCs) modulate MFs excitability by transiently reducing the probability of evoked antidromic spikes (Cabezas et al. 2012). This suggests that GABA release from GCs primarily affects the presynaptic rather than the postsynaptic cellular element.

Here, we show that, in cultured hippocampal autaptic neurons, only GCs expressing glutamic acid decarboxylase-67 (GAD67) show presynaptic $GABA_B$Rs that negatively modulate excitatory postsynaptic current (EPSC) amplitude and tonically activated extrasynaptic $GABA_A$Rs contributing to membrane hyperpolarization under resting conditions. Although these glutamatergic autapses also express functional synaptic $GABA_A$Rs, we never observed any $GABA_A$R-mediated phasic IPSC. We found that GABA coreleased by cultured autaptic GCs specifically activates presynaptic $GABA_B$Rs that reduce the probability of release (Pr) and the readily releasable pool (RRP) size of EPSCs and thus affecting synaptic facilitation, depression, and post-tetanic potentiation (PTP).

Our results suggest that, in addition to its putative role in the functional maturation of adult neuronal circuits (Safiulina and Cherubini 2009; Safiulina et al. 2010) and in preventing excessive postsynaptic depolarization at glutamatergic synapses (Gutiérrez and Heinemann 2001), GABA corelease may also represent an autocrine mechanism to fine-tune the filtering properties of GCs excitatory synapses through a modulation of their short-term plasticity properties.

Results

Inhibitory Markers Are Expressed in a Broad Population of Autaptic Glutamatergic Neurons

Primary cultures of hippocampal autaptic neurons offer the fundamental advantage of recording synaptic currents from isolated neurons, thus activating a defined and homogeneous population of synapses. More importantly, due to the extremely low cell density, they permit to precisely control the extracellular medium surrounding the cell under study (Bekkers and Stevens 1991; Chiappalone et al. 2009), thus avoiding paracrine effects exerted by NTs or other neuromodulators released by neighboring neurons.

Given that the type of NT transporters expressed on SVs (Grønborg et al. 2010) defines the nature of glutamatergic and GABAergic synapses, cultured autaptic neurons (10–15 days in vitro, div) were triple-immunostained for either VGLUT1, VGAT, and GABA or for VGLUT1, GABA, and GAD67 (Fig. 1). On the basis of these experiments, it was possible to identify: 1) pure inhibitory neurons that were immunopositive for VGAT and GABA, but not for VGLUT1 (Fig. 1A, first row); 2) pure excitatory neurons that were positive for VGLUT1, but not for either VGAT or GABA (Fig. 1A, second row) or GABA and GAD67 (not shown); and 3) VGLUT1-positive neurons that also expressed detectable amounts of either GABA and VGAT (Fig. 1A, third row) or GABA and GAD67 (Fig. 1A, fourth row).

When the VGLUT1 expression levels of individual autaptic neurons were plotted against those of VGAT, GABA, or GAD67 (Fig. 1B), 2 distinct populations of neurons could be clearly distinguished, namely 1) autaptic cells characterized by high levels of VGAT, GABA, or GAD67 and the absence (or very low levels) of VGLUT1 (bona fide pure GABAergic neurons) and 2) autaptic cells expressing high or moderate levels of VGLUT1 in parallel with very heterogeneous levels of GABAergic markers, ranging from absence/very low levels (bona fide pure glutamatergic neurons) to medium/high levels. To quantitatively distinguish the latter subpopulation from the other ones, we calculated the product VGLUT1*VGAT (that is enhanced in neurons positive for both markers) and studied the three-dimensional distribution of VGLUT1 and VGAT levels versus VGLUT1*VGAT (Fig. 1C, left). Cluster analysis subsequently applied to the three-dimensional representation separated the third cellular population of autaptic cells coexpressing VGLUT1 together with VGAT (blue symbols; 41% of total neurons) from the populations of pure glutamatergic neurons (red symbols; 35% of total neurons) and pure GABAergic neurons (black symbols; 24% of total neurons), respectively (Fig. 1D). This analysis confirms that a consistent fraction of hippocampal excitatory neurons is potentially able to synthesize and possibly corelease GABA.

The colocalization of VGLUT1 with VGAT or GABA was studied at the level of single synaptic contacts in autaptic glutamatergic neurons (Fig. 2A). The frequency distribution of the immunostained synaptic boutons revealed a high level of colocalization of VGLUT1-positive pixels with VGAT-positive ones (Pearson's coefficient 0.70 ± 0.01, $n = 110$; Fig. 2B, left). As expected from the more widespread distribution of GABA, the colocalization between VGLUT1 and GABA was slightly lower, as shown by the left-shift in the distribution histogram with respect to the VGAT/VGLUT1 distribution (Pearson's coefficient 0.54 ± 0.02, $n = 66$; Fig. 2B, right).

Since many glutamatergic autaptic neurons were found to express GABAergic markers, we next examined whether these cells also coexpress $GABA_A$Rs and $GABA_B$Rs. Neurons were double-stained for VGLUT1 and either $GABA_A\gamma_2$Rs or $GABA_BR_1$s (Fig. 2C). High magnification images of the dendritic trees revealed that both $GABA_A\gamma_2$Rs and $GABA_BR_1$s are expressed at excitatory synaptic terminals and strongly colocalize with VGLUT1 in the majority of excitatory neurons (Fig. 2C), with high levels of the Pearson's coefficient for the $GABA_A$R/VGLUT1 colocalization (0.66 ± 0.14, $n = 133$; Fig. 2D, left) and $GABA_B$R/VGLUT1 colocalization (0.73 ± 0.01, $n = 147$; Fig. 2D, right). These data demonstrate that many glutamatergic synapses are fully equipped with $GABA_A$ and $GABA_B$Rs.

GABA Release at Glutamatergic Autaptic GCs Modulates the Strength of Excitatory Synaptic Currents by Activating Presynaptic $GABA_B$Rs

We then recorded synaptic currents by whole-cell patch-clamp of autaptic neurons obtained from a strain of glutamic acid decarboxylase-green fluorescence protein (GAD67-GFP) knock-in mouse (Tamamaki et al. 2003). The use of these mice offered us the opportunity to identify the expression levels of GAD67 in cultured live neurons before patch-clamp recordings. By this approach,

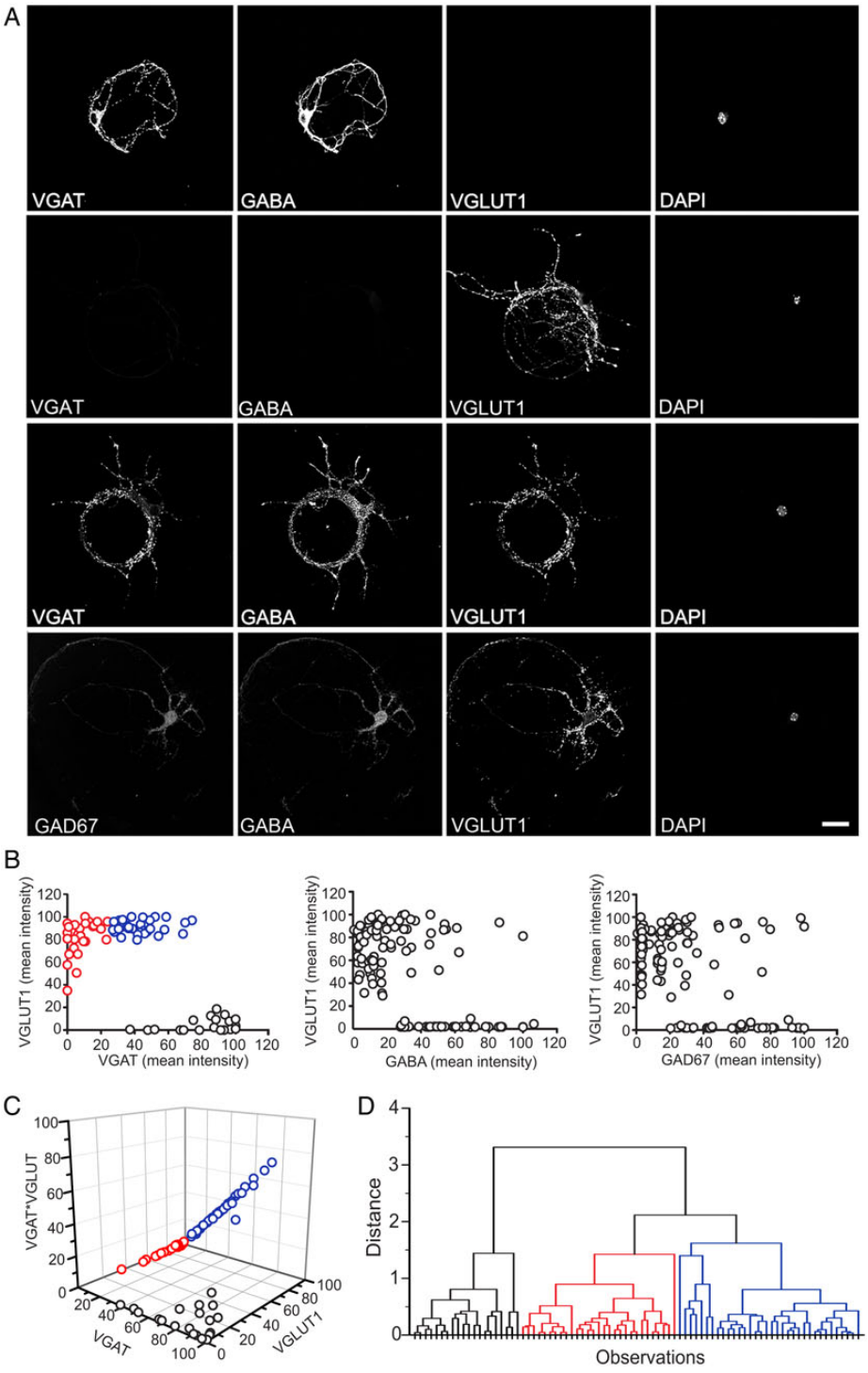

Figure 1. Coexistence of excitatory and inhibitory markers in a broad population of autaptic neurons. (*A*) Representative confocal fluorescence microscopy images of autaptic neurons stained for VGAT, GAD67, GABA, and VGLUT1. From top row to bottom row: an inhibitory autaptic neuron immunonegative for VGLUT1, but positive for VGAT and GABA; an excitatory autaptic neuron immunopositive VGLUT1, but negative for VGAT and GABA; an excitatory autaptic neuron positive for VGLUT1, but also for VGAT and GABA; an excitatory autaptic neuron positive for VGLUT1, but also for GABA and GAD67. Scale bar, 25 μm. (*B*) Distribution of the staining intensities of VGLUT1 versus VGAT, vGLUT1 versus GABA, and VGLUT1 versus GAD67 in the population of autaptic neurons analyzed (each circle represents an individual neuron; $n = 82$, $n = 122$, and $n = 118$ for VGLUT1 versus VGAT, vGLUT1 versus GABA, and VGLUT1 versus GAD67 respectively). The population of inhibitory neurons almost exclusively expressing VGAT, GABA, or GAD67 showed the lowest level of VGLUT1 intensity; pure excitatory neurons almost exclusively expressing VGLUT1 showed low levels of VGAT, GABA, or GAD67 and a consistent percentage of VGLUT1-positive autaptic neurons was also positive for VGAT, GABA, and GAD67. Colors in the left panel refer to the results of the cluster analysis of Panel D. (*C*) Three-dimensional representation of VGLUT1 versus VGAT versus VGLUT1*VGAT from the data presented in B. (*D*) Tree diagram (dendrogram) showing the arrangement in 3 clusters generated by hierarchical cluster analysis applied to the data reported in C (cluster method: group average; distance type: Euclidean).

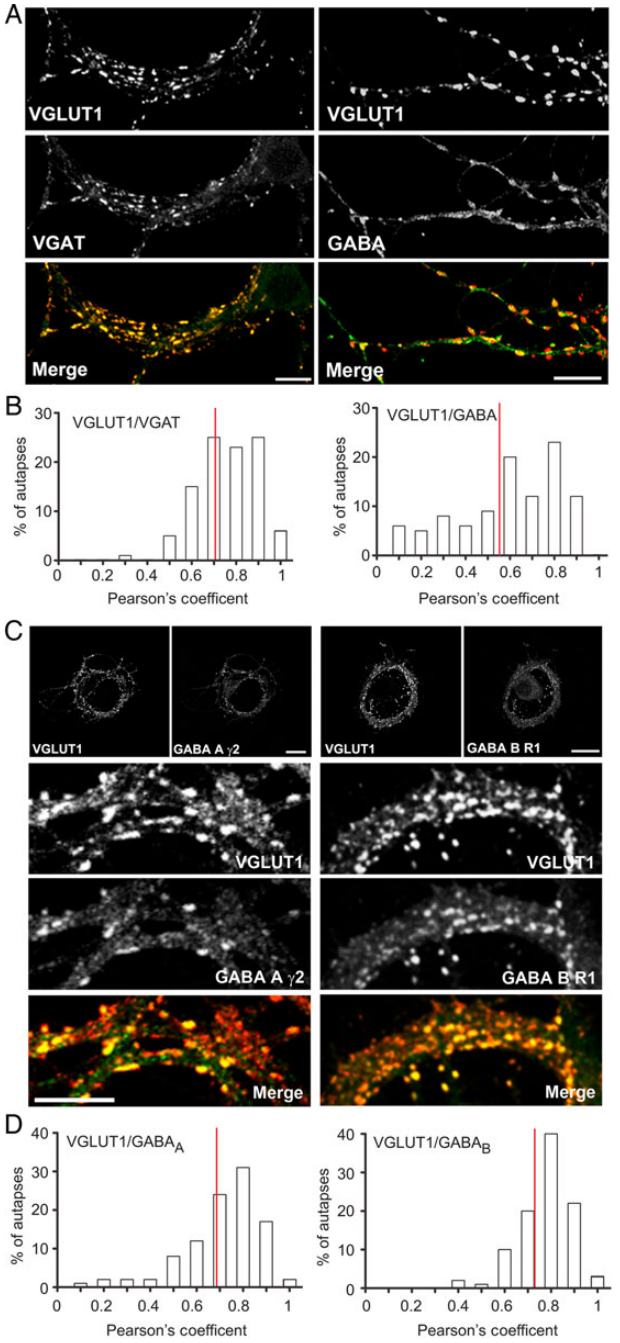

Figure 2. Colocalization of VGLUT1 with inhibitory synaptic markers and GABARs in excitatory autapses. (*A*) Representative images of autaptic contacts positive for VGLUT1 and either VGAT (left panels) or GABA (right panels). The bottom row displays the merge of the VGAT/VGLUT1 or GABA/VGLUT1 channels (scale bar, 10 μm). (*B*) The histograms show the distribution of the Pearson's correlation coefficient values for VGLUT1 and VGAT (left) and VGLUT1 and GABA (right) with respect to the percentage of synaptic puncta analyzed in glutamatergic autaptic neurons. The median value is shown as a red line (0.709 for VGAT/VGLUT1 and 0.5605 for GABA/VGLUT1). (*C*) Representative images of excitatory autaptic neurons immunopositive for VGLUT1 and either $GABA_A\gamma2$ (left) or $GABA_BR1$ (right). Scale bar, 25 μm. (*D*) Higher magnification of VGLUT1-positive autaptic contacts colocalizing with either $GABA_A\gamma2$ (left) or $GABA_BR1$ (right). Scale bar, 10 μm. (*C*) The histograms show the distribution of the Pearson's correlation coefficient values for VGLUT1 and $GABA_A\gamma2$ (left) and VGLUT1and $GABA_BR_1$ (right) with respect to the percentage of synaptic puncta analyzed in glutamatergic autaptic neurons. The median value is shown as a red line (0.696 for $GABA_A\gamma2$/VGLUT1 and 0.737 for $GABA_BR_1$/VGLUT1).

an equal number of cells (13), visually identified as negative, moderately and highly positive to GAD67, have been imaged (Fig. 3Ai–iii images on the left) and successively patch-clamped to analyze their postsynaptic responses. Autaptic neurons were held at −70 mV, and their electrophysiological phenotypes were identified by using specific blockers of excitatory (CNQX, 20 μM) and inhibitory (bicuculline, 30 μM) transmission. We tested the effect of the selective $GABA_BR$ antagonist CGP55845 (CGP 5 μM) on the EPSC amplitude in excitatory autaptic neurons. Each excitatory autaptic neuron was stimulated at 0.1 Hz with a paired-pulse stimulation (inter event interval 50 ms) for over 2 min to obtain a stable baseline before CGP was applied. A first group of autaptic neurons ($n = 13$), chosen for their high positivity to GAD67-GFP, (Fig. 3Aiii, left images) showed slow decaying of post-synaptic currents (PSCs) that were rapidly and completely blocked by bicuculline (Fig. 3Biii). A second group of autaptic cells ($n = 13$) completely negative to GAD67-GFP (Fig. 3Ai, left images) showed fast decaying PSCs that were fully blocked by CNQX and did not respond to the application of the selective $GABA_BR$ antagonist CGP (Fig. 3Bi). On the contrary, a third class of cells ($n = 13$) characterized by a moderate expression of GAD67-GFP (Fig. 3Aii, left images) showed fast decaying glutamatergic PSCs that were fully blocked by CNQX and were significantly enhanced (from 288.3 ± 50.94 to 382.9 ± 68.4 pA, $n = 13$; $P < 0.001$) by CGP application (Fig. 3Bii). The CGP effect on the EPSC amplitude had a rapid progression, reaching a current steady state after less than 1 min of treatment (Fig. 3Bii).

Each patched excitatory neuron was retrospectively analyzed for the expression of Prox1, the selective marker that defines GCs identity (Iwano et al. 2012). The totality (13 of 13) of the GAD67-GFP-negative cells were CGP non-responsive, and 12 of 13 were Prox1 negative (Fig. 3E). On the contrary, all the cells (13 of 13) selected for their moderate positivity to GAD67-GFP were all CGP-responsive and 12 of 13 were Prox1 positive (Fig. 3E).

To further confirm that GABA corelease is present only in autaptic GCs, we also tested the effects of the group II metabotropic glutamate receptor agonist, DCG-IV, in excitatory autaptic cells responsive and non-responsive to CGP treatment. In full agreement with previous results showing that DCG-IV (1 μM) can be used to identify MFs making synapses with CA3 neurons (Kamiya et al. 1996; Beltrán and Gutiérrez 2012), we observed that in CGP-responsive excitatory neurons, DCG-IV inhibited the EPSC, while it was ineffective in CGP non-responsive cells (Supplementary Fig. 1).

These data show that the majority of cultured autaptic GCs diffusely express GAD67 and corelease GABA that modulates the amplitude of EPSC through the activation of $GABA_BRs$. Interestingly, in juvenile mice (p15), GAD67 resulted to be expressed only in a subpopulation of immature GCs (Cabezas et al. 2012), a discrepancy due to higher level of immaturity of the autaptic GCs obtained from mice embryos (E18). Indeed, the Ca^{2+}-binding protein calretinin, a transient marker of the early postmitotic period that characterizes immature GCs (Kempermann et al. 2004), was found in 96.8 ± 2.1 and 96.1 ± 2.9% of the GCs expressing GAD67 in cultured autaptic neurons and low-density neurons, respectively (Supplementary Fig. 2).

Considering the surprisingly high percentage of autaptic GCs that we found under our experimental condition, we compared neuronal-identity in low density and autaptic hippocampal neurons (14–16 div). The percentage of Prox1-positive neurons was significantly lower (~12%) in low-density cultures than that in autaptic neurons (~41%) (Supplementary Fig. 3). Such difference suggests that primary cultures of autaptic hippocampal neurons represent an experimental substrate able to favor the in vitro

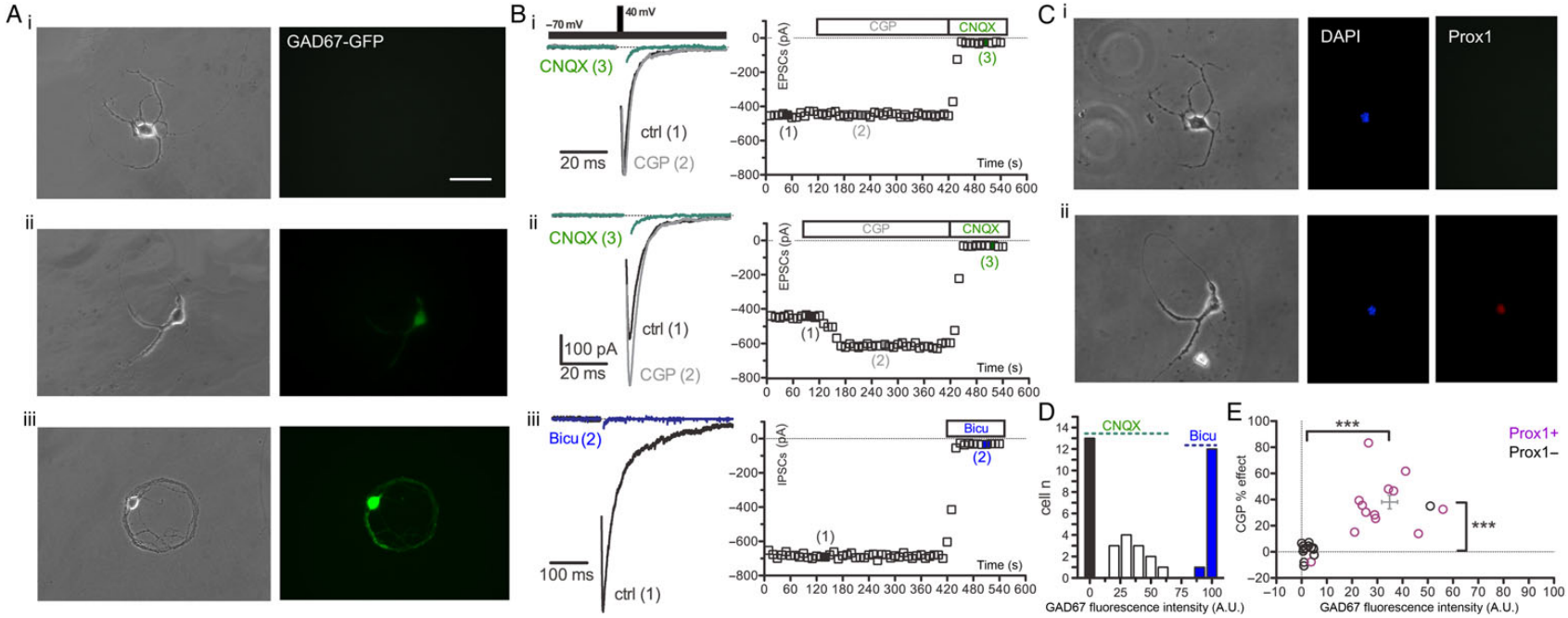

Figure 3. Autaptic GCs expressing GAD67 show tonic inhibition of EPSCs by presynaptic $GABA_BRs$. (Ai–iii) Representative phase-contrast (left) and fluorescent images (right) of cultured (14 div) autaptic neurons obtained from GAD67-GFP knock-in mouse (scale bar, 70 μm). (Bi–iii) Autaptic neurons with different levels of fluorescence were patch-clamped to evoke PSCs that were pharmacologically characterized. The Vh was −70 mV, and the neuron was stimulated with a voltage step to +40 mV lasting 0.5 ms, at a stimulation frequency 0.1 Hz. Representative traces for each tested condition are shown with increasing numbers. Three classes of autaptic neurons were identified based on the GAD67-GFP fluorescence level and the response of PSCs to CNQX, CGP and bicuculline: (Ai,Bi) GAD67-GFP-negative neurons, whose PSCs were insensitive to CGP and fully blocked by CNQX; (Aii,Bii) neurons moderately positive to GAD67-GFP, whose PSCs were enhanced by CGP and fully blocked by CNQX; and (Aiii,Biii) neurons strongly positive for GAD67, whose PSCs were blocked by bicuculline. For each condition studied, the time course of recordings was recorded (right panels). (Ci,ii) Retrospective immunocytochemistry for DAPI and Prox1, a specific nuclear marker for GCs, were performed on non-responsive (Ci) and CGP-responsive excitatory neurons (Cii). To recognize previously patch-clamped neurons, we marked the bottom of the recording chamber just below the neuron with a diamond tip. (*D*) Distribution histogram of the GAD67-GFP fluorescent intensity for the three subpopulations of autaptic neurons visually selected for their different GAD67-GFP intensity. (*E*) Correlation between GAD67-GFP fluorescence intensity and the percent effect of CGP on the EPSC amplitude in Prox1-positive (purple; $n = 13$) and -negative (black; $n = 13$) excitatory autaptic neurons. Each empty dot represents a single cell (Student's unpaired two-tailed *t*-test, $^{***}P < 0.001$).

viability of GCs over other cell-types, thus over increasing their relative abundance.

Characterization of the $GABA_BR$-Mediated Effects of Coreleased GABA on GC Excitatory Synaptic Currents

Characterization of the $GABA_BR$-Mediated Modulation of GC EPSCs due to GABA Corelease

The modulatory action of $GABA_BRs$ on EPSCs was quantitatively dissected in the presence of the selective $GABA_AR$ antagonist bicuculline to identify glutamatergic autaptic neurons and avoid any possible contribution of $GABA_AR$ signaling. Under these conditions, over 60% of the glutamatergic autaptic cells (Fig. 4A; $n = 72$, 46 positives, 26 negatives) displayed ~40% increase of evoked EPSC amplitude in response to CGP (from 242.8 ± 42.4 to 358.4 ± 62.8 pA, $n = 11$; $P < 0.01$; Fig. 4B). The application of paired-pulse stimulation (0.1 Hz, interpulse interval 50 ms; Fig. 4C) to CGP-responsive neurons allowed us to investigate the mechanism of EPSC inhibition by $GABA_BRs$. The treatment with CGP induced a decrease in the paired-pulse ratio (from 2.13 ± 0.16 to 1.49 ± 0.1, $n = 18$; $P < 0.01$; Fig. 4D) which indicates the presynaptic origin of the EPSC enhancement by CGP (Figurov et al. 1996; Gottschalk et al. 1998) and suggests the existence of a presynaptic autocrine inhibition of excitatory terminals coreleasing GABA by GABA-activated presynaptic $GABA_BRs$. To estimate the magnitude of the physiological effect of GABA corelease on the EPSC amplitude, we maximally stimulated presynaptic $GABA_BRs$ at excitatory autapses with acute bath application of exogenous GABA (50 μM) or of the potent and selective $GABA_BRs$ agonist baclofen (20 μM) (Fig. 4E, left and middle traces). Both GABA and baclofen markedly reduced the EPSC amplitude by approximately 60% (57 ± 8%, $n = 12$ and 58 ± 7%, $n = 13$ for GABA and baclofen, respectively; Fig. 4F). On the other hand, the application of CGP on autaptic neurons chronically treated with GABA (1 μM) almost doubled the EPSC amplitude (120 ± 22%, $n = 11$; Fig. 4E, right trace; Fig. 4F). The comparison of the latter result with the ~40% increase of the EPSC amplitude induced by the application of CGP under basal conditions demonstrates that the presynaptic inhibition exerted by GABA release in autaptic GCs represents about one-third of the maximal inhibition reached by full activation of presynaptic $GABA_BRs$.

To exclude the involvement of presynaptic metabotropic glutamatergic receptors in the inhibition of EPSC by $GABA_BRs$, we re-evaluated the CGP effect on the EPSC in the presence of selective antagonists for A1-adenosine receptors (A1Rs) and for the group II/III metabotropic glutamate receptors (mGluR2/3s) DPCPX (1 μM) and LY341495 (4 μM), respectively. When CGP was applied under these conditions, it was still able to induce a significant increase of the mean EPSC amplitude (+42.02%; $P < 0.001$) in ~60% of the tested glutamatergic neurons (Supplementary Fig. 4A,B) and a decrease in PPR (Supplementary Fig. 4C) that were closely similar to those previously observed in the absence of A1R/mGluR2/3 blockade.

GABA could be released synaptically or extra-synaptically by GCs. Indeed, although high-resolution immunogold cytochemistry has shown that both GABA and glutamate are associated with SVs in the same MFTs (Bergersen et al. 2003), it was also reported that GABA can be released extra-synaptically in hippocampal neurons through the reverse action of GABA transporter 1, GAT-1 (Wu et al. 2007). Thus, we examined whether the enhancement of EPSC amplitude evoked by CGP was still present in the presence of the GAT-1 blocker, SKF (50 μM). The percentage of

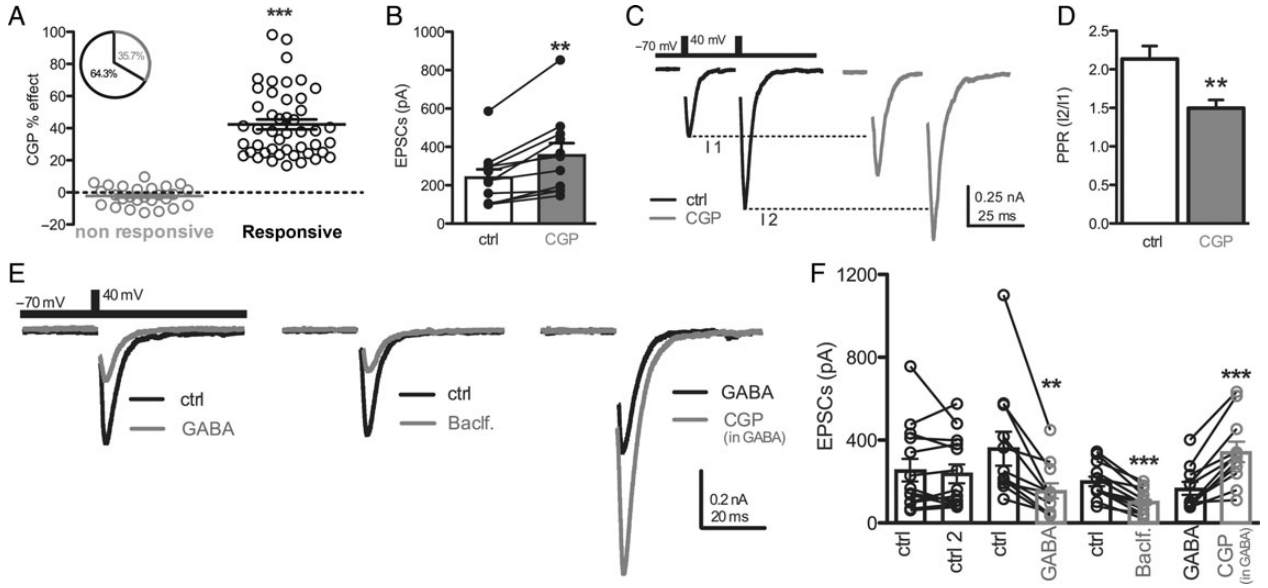

Figure 4. GABA corelease modulates the strength of excitatory autapses through activation of presynaptic $GABA_BRs$. (*A*) Mean (± SEM) percentage increase in EPSC amplitude triggered by CGP application ($n = 72$, 46 positive, 26 negative; Student's unpaired two-tailed *t*-test, ***$P < 0.001$). Neurons displaying at least 10% enhancement of EPSC amplitude were considered CGP-responsive. In the inset, the percentages of responsive (black; 64.3%) and non-responsive (gray; 35.7%) to the CGP treatment are shown. (*B*) Effect of CGP on the mean (±SEM) EPSC amplitude. The superimposed symbols represent the mean EPSCs recorded in individual cells before (ctrl) and after CGP treatment ($n = 11$; Student's paired two-tailed *t*-test, **$P < 0.01$). (*C*,*D*) Representative EPSC traces (*C*) and mean (±SEM) paired-pulse ratio; I_2/I_1; (*D*) showing the effects of a paired-pulse stimulation protocol (interpulse interval 50 ms, 0.1 Hz) administered under control conditions (black trace/empty bar; $n = 18$) or in the presence of CGP (gray trace/bar; $n = 18$; Student's paired two-tailed *t*-test, **$P < 0.01$). The AP artifact was blanked for clarity in all synaptic currents. (*E*) Representative traces showing that the application of GABA (50 μM; left traces) or baclofen (20 μM; middle traces) dramatically inhibits the amplitude of autaptic EPSCs. When CGP (5 μM) was applied on neurons maintained in the presence of GABA (1 μM; right traces), the increase of EPSC was particularly intense. (*F*) Bars represent the mean (±SEM) value of the EPSC amplitude calculated in neurons perfused with control medium and successively treated with GABA, baclofen, or CGP in the presence of GABA. The superimposed symbols represent the mean EPSC values of individual autaptic neurons recorded before and after 10 min of treatment (ctrl–ctrl2, $n = 14$; ctrl–GABA, $n = 12$; ctrl–Baclf, $n = 13$; GABA–CGP in GABA, $n = 12$; Student's paired two-tailed *t*-test, **$P < 0.01$; ***$P < 0.001$).

CGP-responsive cells as well as the increase of the unitary EPSC and the effect on PPR induced by CGP application were virtually unaffected by SKF pretreatment, demonstrating that the reverse action of GAT-1 does not play a role in GABA release in autaptic GCs (Supplementary Fig. 5).

GABA Release in Autaptic GCs Did not Activate Postsynaptic $GABA_BRs$

We also studied whether GABA corelease at autaptic GCs could concomitantly activate postsynaptic $GABA_BRs$ by evaluating whether CGP application is able to change membrane input resistance (Rin) in those cells responding to CGP treatment with an increase of the EPSC amplitude. We injected hyperpolarizing current steps in current-clamp configuration from a holding potential (Vh) of −70 mV to precisely define the Rin under control conditions (Fig. 5A, left traces). Then, we switched to a voltage-clamp configuration to evoke EPSCs in order to test the effect of CGP application (Fig. 5A, middle traces). For the neurons in which CGP increased the EPSC amplitude, we repeated the Rin measurement in the presence of CGP (Fig. 5A, right traces). The Rin was calculated from the slope of the input current/membrane potential relationship (Fig. 5B). We never observed a change of Rin due to GCP application in CGP-responsive cells (Fig. 5C,D), demonstrating that CGP does not act on postsynaptic $GABA_BRs$. Interestingly, in the same cells, also baclofen (20 μM) application did not affect Rin (Fig. 5D). Such lack of function of the postsynaptic $GABA_BRs$ is not surprising in cultured neurons obtained from mouse embryos, as it was previously shown that while $GABA_BRs$ are widely distributed at pre- and post-synaptic sites (López-Bendito et al. 2004), only the presynaptic Rs are functional at birth (Gaiarsa et al. 1995).

GABA Corelease Does not Activate $GABA_A$-Mediated IPSCs

We next investigated whether GABA corelease was able to activate postsynaptic $GABA_ARs$. In an autaptic cell, where CGP was able to enhance EPSCs, the postsynaptic current was blocked by CNQX (20 μM) (Fig. 6A). Under this condition, the residual current was virtually absent and was not further reduced by the application of bicuculline (30 μM; Fig. 6A). This result shows that autaptic glutamatergic synapses coreleasing GABA are postsynaptically silent with respect to $GABA_ARs$, although part of these synapses express $GABA_AR$ clusters (see Fig. 2C,D) that was previously reported to be postsynaptically functional in newborn (Safiulina et al. 2006) and juvenile (Walker et al. 2001; Gutiérrez 2003) MFs-CA3 synapses. Excitatory autaptic neurons (Fig. 6A), where EPSC was fully blocked by CNQX application (Fig. 6B-I) and $GABA_BRs$ inhibited by CGP, were perfused for 120 s with an extracellular solution containing 40 mM K^+ and 100 mM GABA (Fig. 6B-II) and then washed for 30 s. This procedure induces GABA loading into SVs by endocytosis (Bekkers 2005). Indeed, when these neurons were electrically stimulated (60 s after the GABA-loading procedure), an evoked IPSCs (Fig. 6B-III) fully blocked by bicuculline application was apparent (Fig. 6B-IV). This IPSC was characterized by activation and decay kinetics very similar to those of IPSCs evoked in autaptic inhibitory neurons (Supplementary Fig. 6). Moreover, after GABA loading, these excitatory autaptic neurons also showed spontaneous IPSCs blocked by bicuculline application (Fig. 6C). Thus, GABA loading into SVs uncovers normally silent $GABA_AR$ responses in glutamatergic autapses, confirming the expression of functional $GABA_ARs$ observed by immunolabeling studies (see Fig. 2).

Then, we tested whether the $GABA_BR$ inhibitory effect on EPSCs was more effective in neurons whose GABA corelease was increased by the GABA-loading procedure. Indeed, the EPSC exhibited a 50% reduction after GABA loading and a subsequent 2-fold increase when later exposed to CGP (Fig. 6D,E). Both effects resembled the decrease of EPSCs observed after acute treatment with GABA or baclofen, and the CGP-triggered EPSCs increase during chronic GABA treatment, respectively (see Fig. 4F). Then, the amplitude of the $GABA_BR$ effect on EPSCs was compared from the minimal inhibition uncovered by CGP

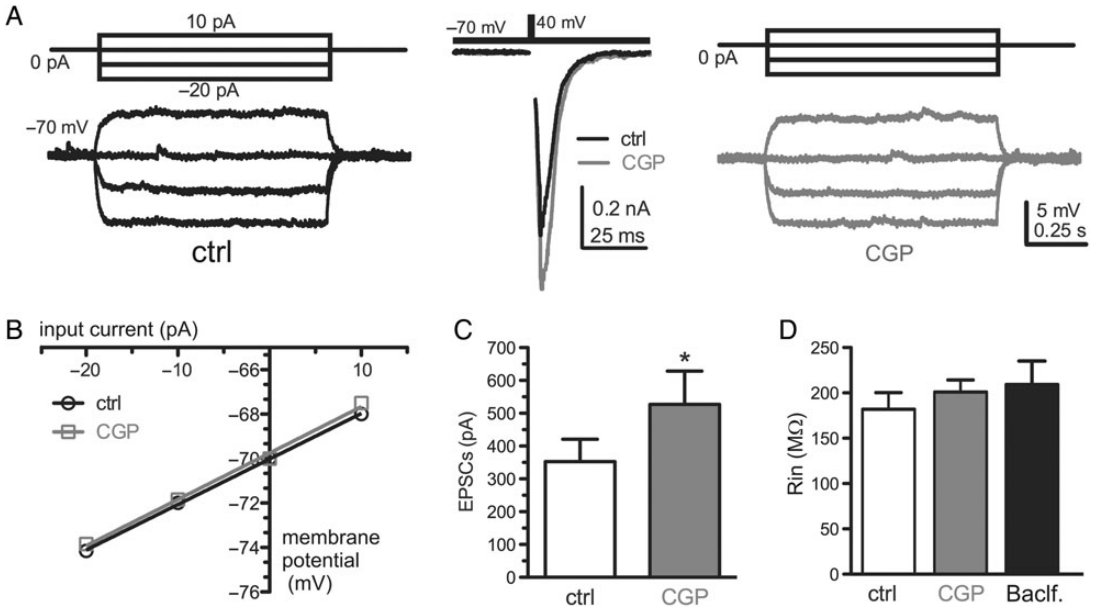

Figure 5. GABA release in excitatory autaptic GCs did not activate postsynaptic $GABA_BRs$. (A) Representative traces showing membrane voltage changes induced by current-steps injection from a Vh of −70 mV before (black traces on the left) and after (gray traces on the right) GCP application, in a GCP-responsive neuron. In the middle panel, the effect of CGP on the EPSC amplitude is shown. (B) Relationship between the input current and the membrane voltage for the same cell shown in A. The Rin was obtained from the slope of the linear regression fitting the data points. (C) The bar graph shows the mean (±SEM) values of EPSC before and after CGP application ($n = 6$; Student's paired two-tailed t-test, $^*P < 0.1$). (D) The bar graph shows the mean (±SEM) values of Rin for the same CGP-responsive cells shown in panel C. The third bar shows the mean (±SEM) value of Rin of autaptic neurons treated with baclofen (20 μM; $n = 6$; one-way ANOVA followed by Bonferroni's test).

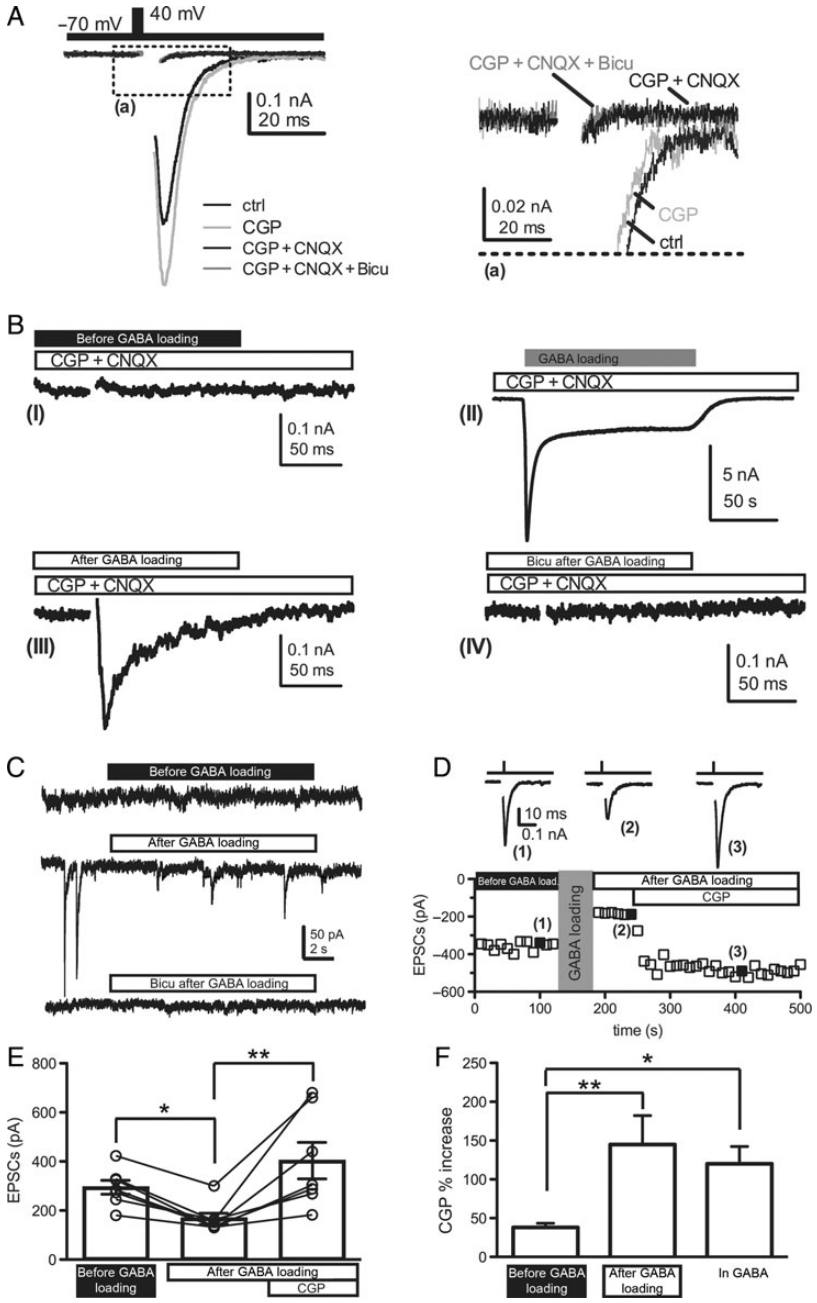

Figure 6. Excitatory autapses express functional presynaptic $GABA_A$Rs that are not activated by GABA corelease. (*A*) The neuron was stimulated with a voltage step to +40 mV lasting 0.5 ms, at a stimulation frequency of 0.1 Hz (Vh = −70 mV). Left: the representative EPSC evoked in an autaptic CGP-responsive cell (recorded in the presence of 50 μM D-APV) was fully blocked by the application of CNQX (20 μM; black trace). The residual current was not affected by application of bicuculline (30 μM). Right: a detail at higher magnification of the residual EPSC after CNQX treatment insensitive to the successive application of bicuculline (30 μM). (*B*) *(I)* EPSC evoked in an autaptic neuron in the presence of CNQX, D-APV, and CGP. *(II)* The same neuron was loaded for 2 min with a solution containing 100 mM GABA, 2 mM $CaCl_2$, and 40 mM KCl. Note the large Cl^- current due to $GABA_A$R activation. *(III)* After GABA loading, the same neuron showed a PSC that was completely blocked *(IV)* by bicuculline (30 μM). (*C*) Representative current traces showing spontaneous synaptic activity recorded (Vh = −70 mV) before (upper trace) and after GABA loading (middle trace). GABA loading induced the appearance of spontaneous IPSCs that were fully blocked by bicuculline (bottom trace). (*D*) Left: representative EPSCs recorded before and after GABA loading in the presence of bicuculline (Traces 1 and 2, respectively) and after addition of CGP (Trace 3). Right: representative time course of the recording described earlier. The neuron was stimulated with a voltage step to +40 mV lasting 0.5 ms, at a stimulation frequency of 0.1 Hz and with Vh = −70 mV. (*E*) Change in the mean (±SEM) EPSC amplitude before GABA loading, after GABA loading, and after GABA loading in the presence of CGP. The superimposed symbols represent the mean EPSCs recorded in individual cells ($n = 7$; Friedman test followed by Dunn's multiple comparison test, $^*P < 0.05$; $^{**}P < 0.01$). (*F*) Mean (±SEM) percent increase in EPSC amplitude induced by CGP before GABA loading ($n = 11$), after GABA loading ($n = 7$), or under chronic GABA (1 μM; $n = 11$; one-way ANOVA followed by Bonferroni's test, $^*P < 0.05$; $^{**}P < 0.01$). In all the plotted synaptic currents, stimulation artifacts were blanked for clarity.

under basal conditions (Fig. 6*F*; right bar) to the maximal inhibition recorded when corelease had been previously boosted by GABA loading of SVs (Fig. 6*F*; middle bar) or by direct activation of $GABA_B$Rs by acute administration of exogenous GABA (Fig. 6*F*; left bar). These results show that the basal inhibition accounts for approximately one-third of the maximal effect.

Overall, the results indicate that GCs autapses express functional $GABA_A$Rs. While the amounts of GABA coreleased at glutamatergic autapses are not sufficient to produce the activation of synaptic $GABA_A$Rs under normal conditions, these GABA concentrations appear to be sufficient to activate presynaptic $GABA_B$Rs and extrasynaptic $GABA_A$Rs, which exhibit a 10-fold higher affinity for GABA than $GABA_A$Rs (Sodickson and Bean 1996).

GABA Release in Autaptic GCs Affects Their Resting Membrane Potential

The tonic inhibition of EPSC by presynaptic $GABA_B$Rs suggests that GABA corelease at GCs could also affect their resting membrane potential (Vrest). As it was well demonstrated that ambient GABA due to synaptic spillover is able to affect neuronal Vrest by activation of extra-synaptic $GABA_A$Rs (Glykys and Mody 2007), we compared the effect that bicuculline application exerts on the Vrest of CGP-responsive and non-responsive excitatory autaptic neurons (Fig. 7*A*). Interestingly, we observed that all the CGP-responsive neurons also responded to bicuculline application with a depolarization of the Vrest (from −61.53 ± 0.95 mV to −56.50 ± 1.31 mV, $n = 6$; $P < 0.001$; Fig. 7*B–D*). On the contrary, in those neurons where the EPSC was insensitive to CGP, the Vrest was not affected by bicuculline application (from −63.62 ± 1.59 to −62.69 ± 1.99 mV, $n = 4$; $P = 0.34$; Fig. 7*C*,*D*). Although we demonstrated that a reverse action of GAT-1 is not involved in GABA corelease (see Supplementary Fig. 5), we considered the possibility the GAT-1 blockade may increase the effect of coreleased GABA on Vrest in CGP-responsive neurons by increasing GABA spillover. To this end, we compared the acute effect of bicuculline on the Vrest of untreated or SKF-89976a (SKF)-treated CGP-responsive cells. As expected, the blockade of GAT-1 activity by SKF (50 μM) induced a significantly larger voltage shift with respect to untreated cells (from 5.033 ± 0.67, $n = 6$ to 6.75 ± 0.31 mV, $n = 8$; $P < 0.05$; Fig. 7*E*). The latter result demonstrates that the modulation of Vrest by coreleased GABA is particularly sensitive to inhibition of GABA reuptake, while the activation of presynaptic $GABA_B$Rs seems to be relatively independent of GAT-1 activity.

GABA Corelease Modulates the Quantal Properties of Release

The main presynaptic factors controlling synaptic strength are the Pr and the size of the RRP of SVs (Zucker and Regehr 2002). Recent data obtained at the calix of Held synapse (Thanawala and Regehr 2013) showed that the inhibition of presynaptic Ca^{2+} influx through the activation of $GABA_B$Rs reduced both Pr and the synchronous RRP size (RRP_{syn}). To evaluate the effects of GABA corelease on these parameters, we analyzed the cumulative amplitude profile during high-frequency stimulation (HFS: 40 Hz train for 1.5 s; Schneggenburger et al. 1999; Baldelli et al. 2005, 2007; Medrihan et al. 2013) (Fig. 8*A*). Although we noticed that CGP also increased the asynchronous component of release, we limited our analysis to the synchronous release, knowing that the RRP_{syn} determined with this method is an underestimation of the total RRP size composed of both synchronous and asynchronous pools of SVs (Moulder and Mennerick 2005; Stevens and Williams 2007; but see also Medrihan et al. 2013).

To ensure the accuracy of our estimation of Pr and RRP_{syn} size changes in CGP, the quantal size was determined in each CGP-responsive autaptic neuron before and 10 min after the application of CGP. No differences in the amplitude of mEPSCs that occurred either spontaneously or after a 0.25-s train at 50 Hz were found (10.00 ± 0.44 and 10.01 ± 0.40 pA before and after CGP, respectively, $n = 8$; $P = 0.98$; data not shown), testifying the substantial preservation of the quantal size.

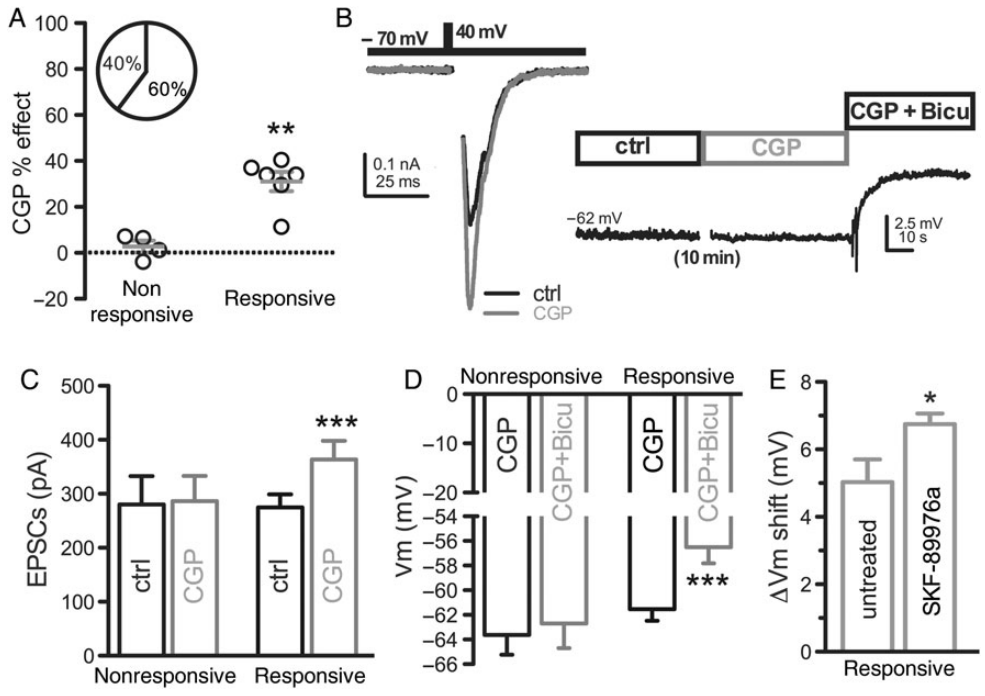

Figure 7. GABA release at autaptic GCs activates extrasynaptic $GABA_A$Rs that maintain the resting potential hyperpolarized. (*A*) In 6 of 10 autaptic cells, GCP increased the amplitude of eEPSC. (*B*) Example of CGP-induced increase of the eEPSC amplitude. In the same cell, the application of bicuculline (30 μM) depolarized the Vrest measured in current-clamp configuration. (*C*) The bar graph represents the mean (±SEM) values of eEPSCs amplitude before and after CGP application in CGP non-responsive ($n = 4$) and responsive cells ($n = 6$, Student's paired two-tailed *t*-test, ***$P < 0.001$). (*D*) The bar graph shows the mean (±SEM) Vrest values before and after bicuculline application in CGP non-responsive ($n = 4$) and responsive cells ($n = 6$, Student's paired two-tailed *t*-test, ***$P < 0.001$). (*E*) The bar graph shows the mean (±SEM) Vrest shift induced by bicuculline in untreated ($n = 6$) and SKF-89976a-treated CGP-responsive cells ($n = 8$, Student's unpaired two-tailed *t*-test, *$P < 0.05$).

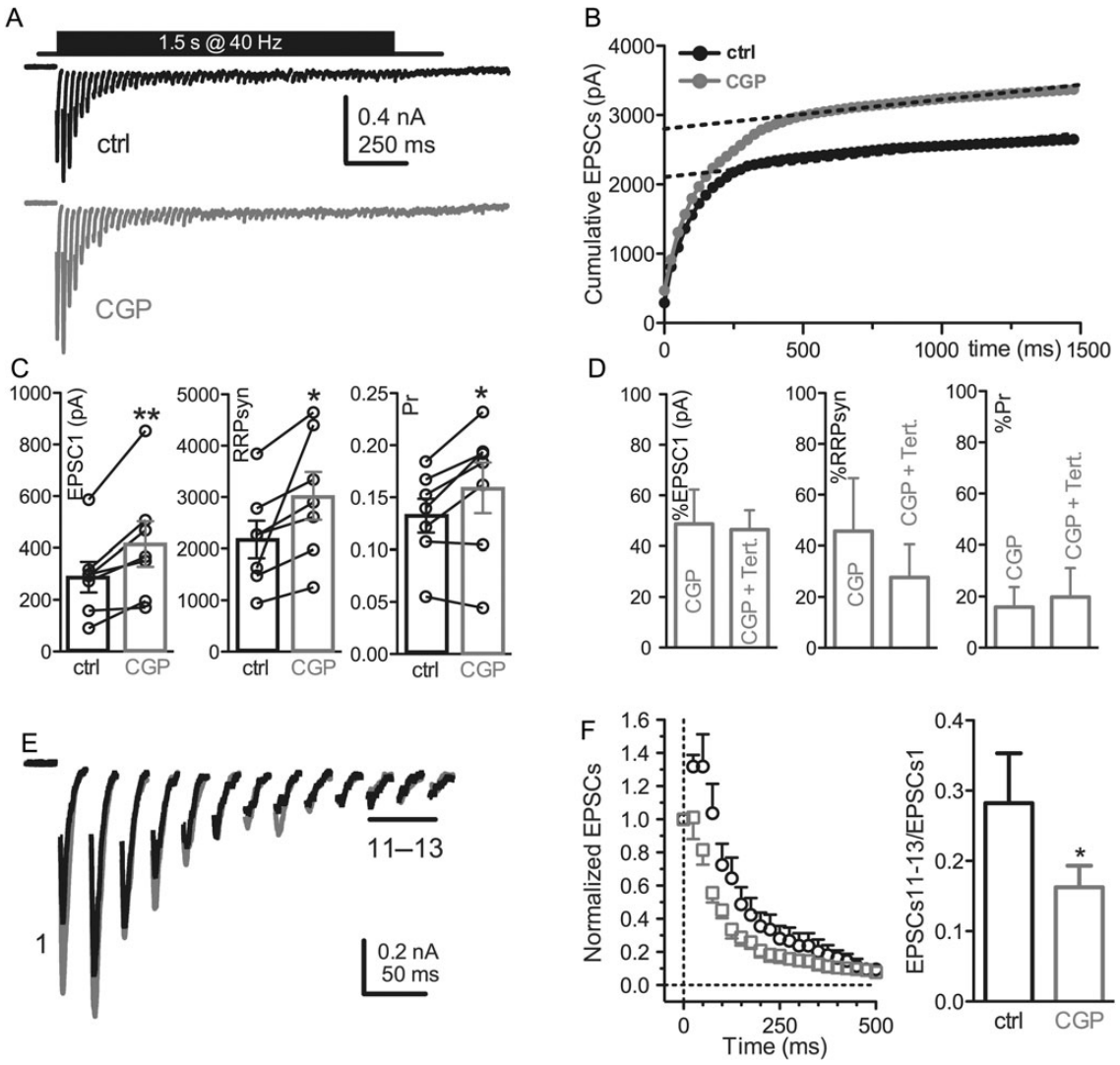

Figure 8. GABA corelease alters quantal parameters of excitatory autapses through presynaptic $GABA_BR$ activation. (*A*) Representative recordings of EPSCs evoked by a short HFS (1.5 s at 40 Hz) under control conditions (black trace) and after 10 min of treatment with CGP (gray trace). Stimulation artifacts were blanked for clarity. (*B*) Cumulative amplitude profiles for a representative autaptic cell under control conditions (black symbols) and after CGP treatment (gray symbols). Data points in the range 0.5–1.5 s were fitted by linear regression and back-extrapolated to time 0 (dashed lines) to estimate the RRP size. (*C*) Bars represent the mean (±SEM) amplitude of the first EPSC in the train ($EPSC_1$; left), RRP_{syn} size (center), and Pr (right) estimated under control conditions (black bars; $n = 7$) and after CGP treatment (gray bars; $n = 7$). Symbols superimposed to the bars represent the parameters of individual neurons before and after the treatments (Student's paired two-tailed *t*-test, $^*P < 0.05$; $^{**}P < 0.01$). (*D*) Comparison of the mean (±SEM) percent change of the first EPSC in the train ($EPSC_1$; left), RRP_{syn} size (center), and Pr (right) induced by CGP in control cells (same data shown in panel C) and in cells pretreated with tertiapin-Q (50 nM), a blocker of GIRKs ($n = 7$; Student's unpaired two-tailed *t*-test). (*E*) Representative current traces showing the first 13 EPSCs evoked during HFS under control conditions (black) and after application of CGP (gray). (*F*) Plots of normalized mean (±SEM) eEPSC amplitude versus time during repetitive stimulation (0.5 s at 40 Hz) of autaptic neurons before (black symbols; $n = 7$) and after (gray symbols; $n = 6$) CGP treatment. Bars represent the mean (±SEM) ratio of the averaged amplitude of the 11th, 12th, and 13th EPSCs, normalized to the first EPSC of the HFS under control conditions (black bars; $n = 7$) and after CGP treatment (gray bars; $n = 7$; Wilcoxon Matched-pairs test).

During the trains, a significant depression of EPSCs became apparent and the cumulative profile of repeated EPSC amplitude showed a rapid rise followed by a slower linear increase of various steepness at later pulses (Fig. 8A,B). Assuming that the slow linear rise is attributable to the equilibrium between the release-induced depletion and the constant replenishment of the RRP at a Pr approaching 1.0 during the train, the back-extrapolation of the linear portion to time 0 yields a rough estimation of the total release minus the total replenishment, corresponding to the size of RRP_{syn} (Schneggenburger et al. 1999). As shown in Figure 8C, RRP_{syn} was significantly increased by CGP treatment (from 2173 ± 360 to 3019 ± 464 pA, $n = 7$; $P < 0.05$) to a similar extent of the increase in amplitude of the first EPSC in the train (from 288 ± 58 to 415 ± 87 pA, $n = 7$; $P < 0.01$). The SV release probability Pr, calculated as the ratio between I_1 and RRP_{syn} (see Materials and Methods), was also significantly increased by CGP (from 0.132 ± 0.01 to 0.158 ± 0.046, $n = 7$; $P < 0.05$; Fig. 8C). Thus, the increase of EPSC amplitude, obtained by removing the tonic $GABA_B$-R-mediated inhibition exerted by GABA corelease, results from a combined increase in RRP size and Pr of synchronous release.

It has recently been reported (Cabezas et al. 2012) that $GABA_BRs$ activation by endogenous GABA primarily affects axonal MF excitability through modulation of G protein-coupled inwardly rectifying K^+ channels (GIRKs) in juvenile (P10–20)

mice. To evaluate whether this process could play a role in the CGP effect on RRP size and Pr, we treated neurons with the high-affinity GIRKs antagonist tertiapin-Q (50 nM). The CGP-induced enhancement of RRP size and Pr was not affected by the GIRK antagonist (Fig. 8*D*), ruling out an involvement of GIRKs in this effect.

The dynamics of synaptic depression of glutamatergic autapses induced by a short (0.5 s) HFS (40 Hz) was also investigated. CGP-responsive autaptic GCs exposed to control medium showed a rapid increase in the EPSCs amplitude during the first 2 stimuli of the short train followed by a stepwise reduction to a steady state (Fig. 8*E*,*F*). The time course of EPSC amplitude, normalized to the amplitude of the first stimulus of the train, revealed that CGP application abolished synaptic facilitation during the first part of the train. Moreover, CGP increased the synaptic depression calculated as the ratio between the average amplitude of the 11th, 12th, and 13th EPSCs normalized to the first EPSC of the HFS (Fig. 8*E*,*F*). These results clearly demonstrate that, in autaptic GCs, a tonic activation of presynaptic $GABA_BRs$ due to GABA corelease increases facilitation and reduces depression limiting SV depletion during HFS via a down-regulation of Pr and RRP_{syn}.

GABA Corelease Modulates Post-tetanic Potentiation at Glutamatergic Autapses through Presynaptic $GABA_BRs$ Activation

Sustained synaptic activity, mimicked by a brief HFS, induces PTP of EPSCs in glutamatergic autaptic neurons. This form of short-term plasticity is contributed by an increase in Pr due to intraterminal Ca^{2+} buildup and a parallel increase in the RRP size due to enhanced SV mobilization (Zucker and Regehr 2002; Valente et al. 2012).

A short HFS (1.5 s at 40 Hz; Fig. 9*A*) was administered, and a single-pulse stimulus was applied 10 s after the end of the train to estimate the maximal percent increase of EPSC amplitude with respect to the basal EPSC amplitude before the train (PTP_{max}). Then, single-pulse stimuli were continuously applied at 0.1 Hz for 150 s to monitor the temporal decay of PTP and the return of EPSCs to the basal amplitude (Fig. 9*B*). While CGP-responding autapses exposed to control medium showed a PTP of 100% (Fig. 9*C–E*), they exhibited an impaired PTP with a potentiation of only about 60% when the same autaptic neurons were treated with CGP (Fig. 9*C–E*). These results suggest that PTP in control medium is higher because the $GABA_BR$-mediated tonic inhibition keeps the basal Pr and RRP size low. When such inhibition is removed by CGP, the pre-train Pr and RRP values increase and the

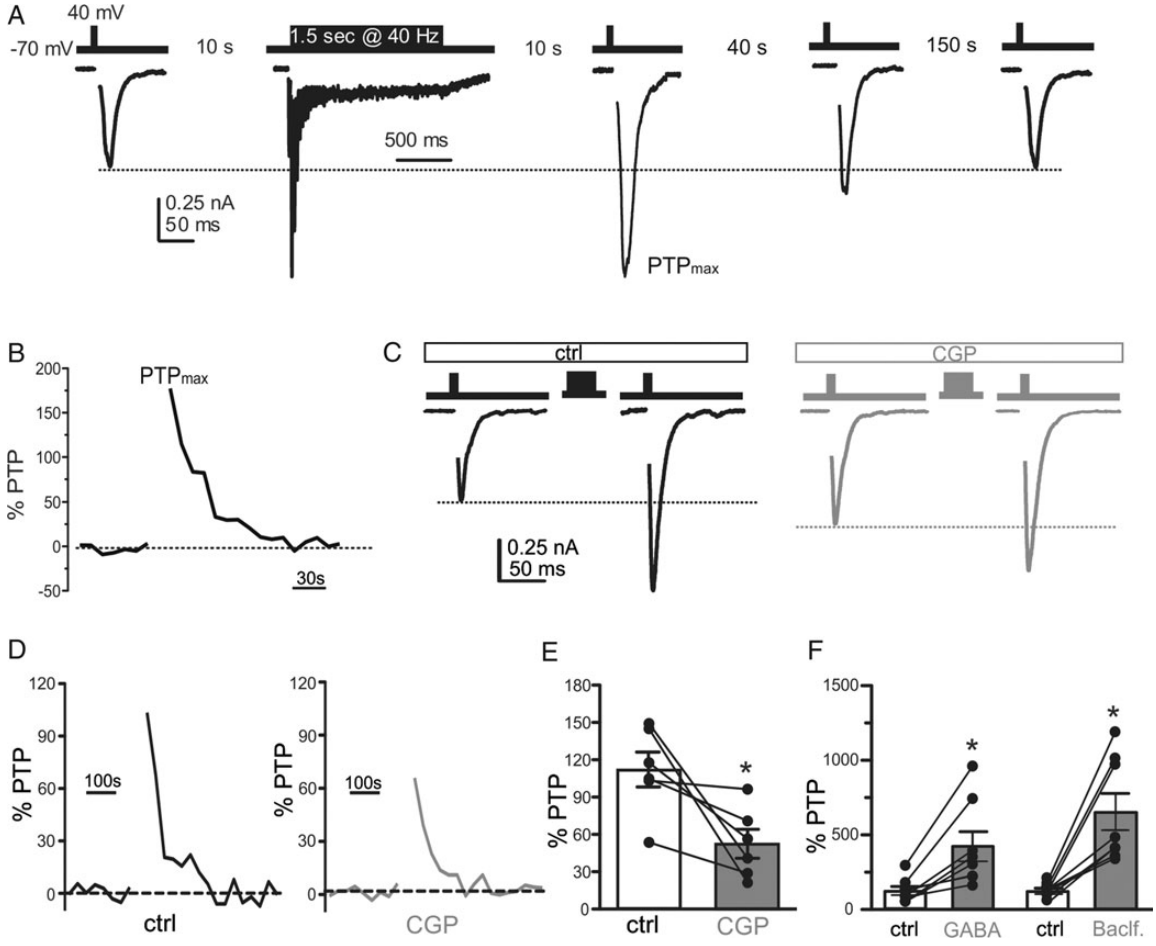

Figure 9. GABA corelease modulates PTP. (*A*) The experimental protocol used to investigate PTP was based on single stimuli applied at basal stimulation frequency (0.1 Hz) followed by a train of 1.5 s at 40 Hz, resumed, and repeated until the EPSC amplitude returned to the pre-train level. (*B*) The maximal PTP (PTP_{max}) was observed 10 s after the train and the EPSC amplitude quickly recovered the baseline value within 150 s. (*C*,*D*) Representative traces (*C*) showing EPSCs before and after tetanic stimulation and time courses of PTP (*D*) for neurons incubated under either control (black) or CGP (gray) conditions. PTP was calculated as the percent increase in eEPSC amplitude with respect to the average EPSC amplitude before the train. (*E*,*F*) Bars (means±SEM) represent the amplitude of maximum PTP expressed as the percentage increase with respect to the mean baseline EPSC. Superimposed symbols show PTP changes observed in individual autaptic cells ($n = 14$ for all conditions; Student's unpaired two-tailed *t*-test, $^{**}P < 0.01$).

magnitude of PTP decreases. Thus, in cultured autaptic GCs, the presence of a tonic presynaptic $GABA_BRs$-mediated inhibition due to GABA corelease modulates the expression of synaptic facilitation, depression, and PTP by adjusting Pr and RRP size values.

Interestingly, PTP increased from ≈100% to ≈400 or ≈600% when autaptic GCs under control conditions were stimulated with GABA (50 μM) or baclofen (20 μM), respectively (Fig. 9F). This result clearly confirms (see Fig. 7F) that the level of activation of $GABA_BRs$, due to GABA corelease, is far from being saturated and can be considerably increased during sustained tetanic stimuli through the progressive buildup of coreleased GABA.

Presynaptic $GABA_BR$ Activity Dynamically Modulates the Strength and Filtering Properties of Glutamatergic Synapses

Short-term plasticity is believed to have a central role in synaptic computation in neural circuits (Abbott and Regehr 2004). In this context, synapses can perform various types of temporal filtering operations by converting patterns of action potentials (APs) into distinct postsynaptic responses (Dittman et al. 2000). We have shown that $GABA_BRs$ activation by coreleased GABA allows autaptic GCs to fine-tune the probability of glutamate release. To evaluate the consequences of this autocrine modulation on the dynamics and filtering properties of autapses, we elicited EPSCs by a short train of 13 stimuli administered at stimulation frequencies ranging between 0.01 and 50 Hz (Fig. 10A).

The average amplitude of the last 3 EPSCs, normalized to the first EPSC of the train, was plotted as a function of the stimulus frequency both under control conditions and when $GABA_BRs$ were activated by baclofen or blocked by CGP (Fig. 10B). Under control conditions, CGP-responding excitatory autapses did not show any depression at stimulation frequencies equal or below 0.1 Hz, whereas a clear depression appeared at higher frequencies that progressively increased with the frequency. Application of CGP significantly enhanced the steady-state depression (Fig. 10B, upper panel; from 0.2 ± 0.02 to 0.1 ± 0.02 at 50 Hz, $n = 10$; $P < 0.001$), and baclofen greatly reduced it (Fig. 10B, lower panel; from 0.21 ± 0.03 to 0.66 ± 0.1 at 50 Hz, $n = 10$; $P < 0.001$) at frequencies higher than 0.1 Hz. The data indicate that the stimulation of $GABA_BRs$ by coreleased GABA (compare the EPSC ratio profiles under control and CGP conditions) becomes clearly detectable at stimulation frequencies above 1 Hz. Considering that the maximal presynaptic modulation exerted by $GABA_BRs$ corresponds to the difference between the EPSC ratio profiles in baclofen and CGP, the endogenous stimulation of $GABA_BRs$ by coreleased GABA accounts for a moderate, but significant, receptor occupancy.

To better understand the consequences of $GABA_BR$ modulation due to GABA corelease on the dynamic behavior of synaptic responses, EPSCs were recorded during a Poisson stimulation pattern, i.e., during an irregular stimulation train lasting 5 s with an average rate of 20 Hz (a detail of the Poisson stimulation lasting 1 s is shown in Fig. 10C). Using a current threshold (I_t) value corresponding to the 70% of the maximal EPSC amplitude evoked during the Poisson stimulation, we evaluated the theoretical probability of each EPSC to evoke an AP (i.e., the probability that an EPSC exceeds the I_t; Fig. 10C). The probability to evoke an AP observed under control conditions was markedly reduced during the high-frequency bursts and was followed by a clear recovery at inter-spike intervals longer than a few hundreds of milliseconds (Fig. 10D, black trace). As predicted, synapses favored the transfer of APs from the presynaptic terminal to the postsynaptic side at low stimulation frequencies, whereas they blocked AP propagation at higher frequencies, working as a low band-pass filter (Fig. 10D, black trace). The AP probability in the high-frequency band was further reduced by CGP treatment due to its capability to enhance synaptic depression (Fig. 10A–C, D, dark gray traces). This effect demonstrates that the complete removal of the $GABA_BR$ inhibition exacerbates the low band-pass filtering properties of excitatory synapses. On the contrary, baclofen, by reducing synaptic depression, favored the AP propagation at higher frequencies (Fig. 10A–D, light gray trace), switching the synapses toward a higher band-pass mode. These results indicate that GABA corelease at glutamatergic autapses confers tunable active properties with a high dynamic range for band-pass filtering through a use-dependent presynaptic modulation of the quantal release parameters.

Discussion

Over the past 2 decades, several reports have shown that peptides are coreleased with classical NTs (for a recent review, see Hnasko and Edwards 2012). However, an increasing amount of recent evidence has demonstrated that also classical transmitters can be coreleased at central synapses (Jonas et al. 1998; Li et al. 2004). One of the most puzzling cases is GABA corelease at glutamatergic synapses, which has been observed in GCs of the dentate gyrus in juvenile animals (Walker et al. 2001; Gutiérrez et al. 2003; Safiulina et al. 2006; Beltrán and Gutiérrez 2012; Cabezas et al. 2012) or in the adulthood after epileptic discharges (Sloviter et al. 1996; Gutiérrez and Heinemann 2001; Gutiérrez 2000). Although MFTs have been shown to contain GABA (Sandler and Smith 1991; Bergersen et al. 2003), GAD (Sloviter et al. 1996) and GAT1 (Zander et al. 2010), the functional role of GABA release at juvenile MFTs is still debated.

Here, we show that, in hippocampal autaptic neurons obtained from mouse embryos (E18), a high percentage of glutamatergic neurons show molecular evidence of a GABAergic phenotype. Patch-clamp recordings revealed that a large proportion of glutamatergic autaptic neurons (~60%) expressing a moderate level of GAD67 also responded to CGP with an increase of the EPSC. On the contrary, excitatory autaptic neurons fully negative for GAD67 were non-responsive to CGP. Retrospective immunocytochemistry that followed patch-clamp recordings revealed that all the CGP-responsive excitatory autaptic neurons were GCs positive to the specific marker, Prox1.

The vast majority of previous studies investigating GABA corelease at MFTs were looking for the presence of $GABA_AR$ responses, and a similar functional characterization was never performed in depth in autaptic hippocampal neurons. In agreement with a previous report (Cabezas et al. 2012), we never observed phasic $GABA_AR$ responses in autaptic GCs under control conditions, whereas autaptic IPSCs due to the activation of postsynaptic $GABA_ARs$ were observed only after the GABA-loading procedure. However, we observed that all the CGP-responsive neurons also responded to bicuculline application with a Vrest depolarization, demonstrating that GABA release in GCs activates a tonic hyperpolarizing current probably due to extrasynaptic $GABA_ARs$ activation. Although functional $GABA_A$ and $GABA_BRs$ were both expressed at autaptic GCs, it is likely that the low amount of coreleased GABA may be only sufficient to activate extrasynaptic $GABA_ARs$ and presynaptic $GABA_BRs$ due to their higher affinity for GABA with respect to postsynaptic $GABA_ARs$ (Sodickson and Bean 1996; Semyanov et al. 2004). However, we cannot exclude that the amount of postsynaptic $GABA_A$-Rs expressed at these primarily excitatory synapses is not adequate to evoke a detectable autaptic IPSC under normal conditions.

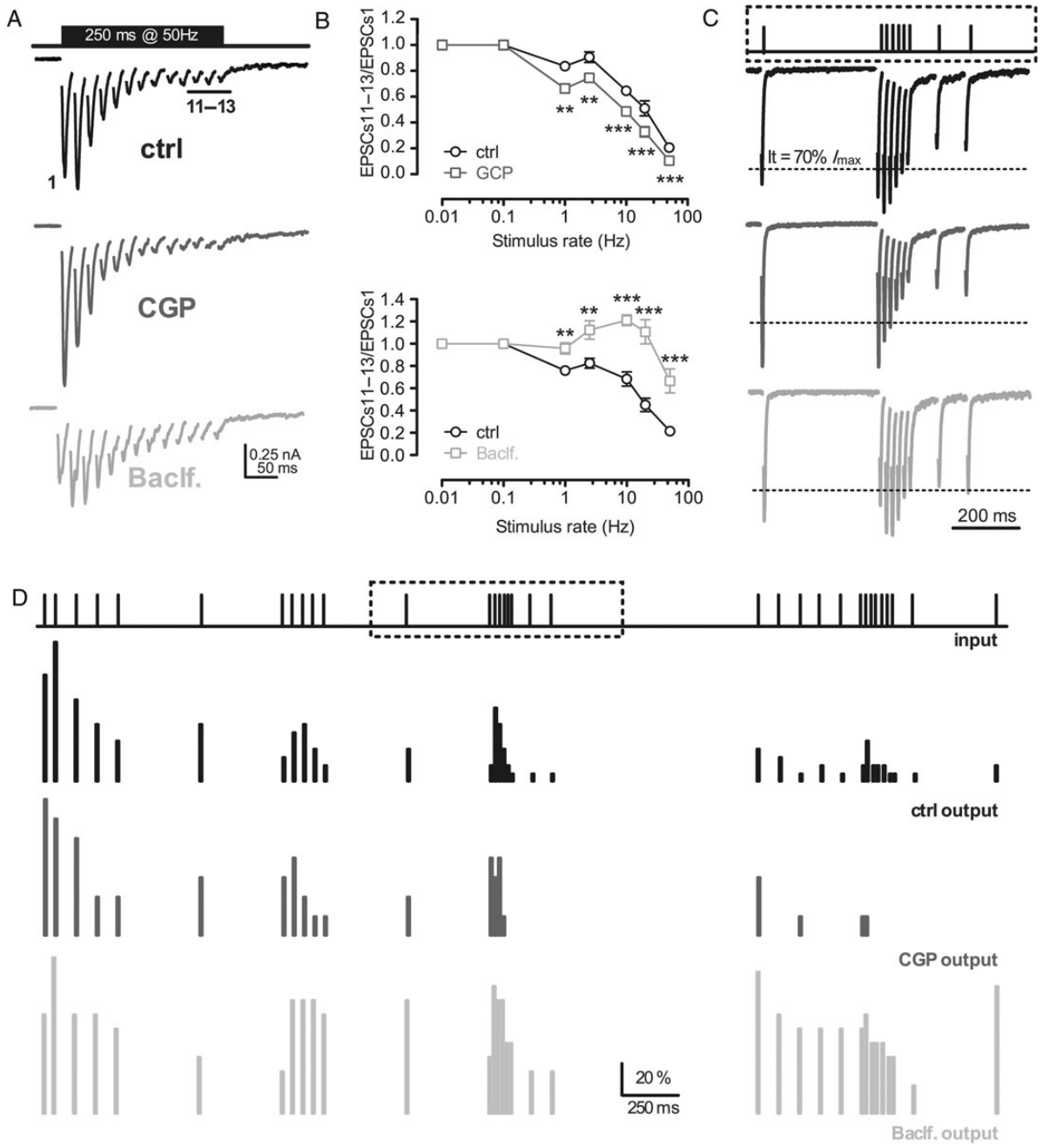

Figure 10. GABA corelease dynamically modulates the filtering properties of glutamatergic autapses. (*A*) Representative EPSCs evoked by short train stimulation (250 ms at 50 Hz, inset) under control conditions (black trace) or after 10 min treatment with either CGP (dark gray trace) or baclofen (light gray trace). Stimulation artifacts were blanked for clarity. (*B*) Average amplitude of the last 3 EPSCs in the train divided by the amplitude of the first EPSC and plotted as a function of the stimulation frequency (0.01, 0.1, 1, 2.5, 10, 20, and 50 Hz) under control conditions (black traces/symbols; $n = 10$), in the presence of CGP (dark gray traces/symbols; $n = 10$), or in the presence of baclofen (light gray traces/symbols; $n = 10$). Data are shown as means±SEM; Student's unpaired two-tailed *t*-test, $^{**}P < 0.01$; $^{***}P < 0.001$. (*C*) Representative time window of 1 s showing EPSCs evoked by a Poisson stimulation (random stimulus train lasting 5 s at an average rate of 20 Hz, top) applied under control conditions (black trace), in the presence of CGP (dark gray trace), or in the presence of baclofen (light gray trace). Each EPSC trace is obtained by averaging 4 trials repeated at 20-s intervals. Stimulation artifacts are blanked for clarity. The current threshold was placed at the 70% of the maximal EPSC (I_{max}) evoked during the Poisson stimulation. (*D*) Time course of the average probability that a single EPSC, evoked during the Poisson stimulation, overtakes the current threshold (70% of the I_{max}) under control conditions (black, $n = 14$), after CGP (dark gray, $n = 6$), or after baclofen (light gray, $n = 8$).

The effect of the endogenous GABA corelease on glutamatergic transmission was uncovered by the significant enhancement of EPSC amplitude (from 242.81 ± 42.42 to 358.45 ± 62.88 pA, $n = 11$; $P < 0.01$) coupled to a decreased PPR in response to the application of CGP (from 2.13 ± 16 to 1.49 ± 0.1, $n = 18$; $P < 0.01$), a selective $GABA_BR$ antagonist. These results indicate that the endogenous activation of $GABA_BRs$ by coreleased GABA causes a decrease of Pr that is likely to occur through Gβγ-mediated inhibition of voltage-gated Ca^{2+} channels (Wu and Saggau 1995; Dittman and Regehr 1996) and activation of K^+ channels that shunt the AP and

limit the presynaptic Ca^{2+} influx (Thompson and Gähwiler 1992). Interestingly, we and others (Thanawala and Regehr 2013) also found that CGP increases the RRP size, indicating that $GABA_BRs$ also influence SV trafficking by decreasing the availability and/or the priming of SVs for release. These additional effects of $GABA_BR$ activation by coreleased GABA may be mediated by the inhibition of adenylyl cyclase by $G\alpha_i/G\alpha_o$ subunits (Sakaba and Neher 2003; Rost et al. 2011) or be the consequence of the decreased activation of CaM kinases I/II and synapsin phosphorylation by the reduced Ca^{2+} influx (Cesca et al. 2010).

Cultured autaptic neurons represent an artificial system and for this reason results based on this specific experimental substrate need to be considered cautiously. In particular, it was previously reported (Rao et al. 2000) that pyramidal excitatory autaptic neurons form clusters of $GABA_ARs$ in the absence of GABAergic inputs. These $GABA_ARs$ clusters facing glutamatergic terminals have been interpreted as a mismatch, possibly reflecting a common signal involved in the alignment of pre- and postsynaptic components during the formation of excitatory and inhibitory synapses (Rao et al. 2000). However, in a more physiological system such as acute hippocampal slices, the MFTs showed colocalization of AMPA and $GABA_ARs$ (Bergersen et al. 2003), and the functionality of these $GABA_ARs$ has been widely proved by electrophysiological studies (Walker et al. 2001; Gutiérrez et al. 2003; Safiulina et al. 2006).

Moreover, cultured glutamatergic autaptic neurons represent a simplified in vitro model of neuronal hyperexcitability due to the reverberant action of their excitatory autapses that produce periods of bursting discharges. Under these conditions, GABA corelease could represent a homeostatic mechanism preserving neurons from excessive hyperexcitability. A similar functional role has been postulated for GABA corelease at MFTs in the CA3 region of the adult hippocampus during epilepsy (Gutiérrez and Heinemann 2001; Treviño and Gutiérrez 2005; Gutiérrez and Heinemann 2006; Treviño et al. 2007; Gutiérrez 2009). In this hippocampal area, an altered sprouting and synaptic reorganization of MF axons has been observed in human temporal lobe epilepsy and in various animal models of epilepsy, including kindling (Nadler 2003). Intense activation of MFs, both in vitro and in vivo, results in increased levels of GAD67 and VGAT mRNAs in GCs of the dentate gyrus, which allow GABA to be released from MFTs on CA3 pyramidal cells (Schwarzer and Sperk 1995; Sloviter et al. 1996; Gutiérrez 2000). Interestingly, GABA is coreleased also by MFTs that make synapses onto interneurons targeting CA3 pyramidal cells (Romo-Parra et al. 2003; Safiulina et al. 2006). However, it has been shown (Gutiérrez and Heinemann 2001; Treviño et al. 2007) that, although pyramidal cells and interneurons receive the same dual MF input, the ratio of the glutamate/GABA release is higher in interneurons than that in pyramidal cells. Thus, inhibition overrides excitation in CA3 pyramidal neurons, contrarily to what happens in interneurons.

An important concern in the evaluation of the functional impact of our data is that all the evidence suggesting that GABA corelease represents a protective mechanism to preserve neuronal network from hyperexcitability has been observed in adult animals. On the contrary, our data derive from cultured autaptic neurons, obtained from E18 mouse embryos and recorded after 10–15 days of in vitro maturation. Cultured neurons of this age, although electrophysiologically functional (Bekkers and Stevens 1991), are probably still in a postnatal developmental phase. Indeed, we detected, in Prox1/GAD67-positive GCs, the Ca^{2+}-binding protein, calretinin (Supplementary Fig. 2), a key marker of an early postmitotic stage of immature GCs, that is later exchanged for the mature GC marker calbindin (Kempermann et al. 2004). Previous results showed that before P10, GCs of the dentate gyrus express GAD67 and VGAT mRNAs and produce EPSPs that are blocked by bicuculline (Gutiérrez et al. 2003; Maqueda et al. 2003; Safiulina et al. 2006). At later stages, GABA becomes hyperpolarizing (Gutiérrez et al. 2003) and, by P22-P23, VGAT and GAD67 mRNAs dramatically decline and no further $GABA_A$ currents are detected (Gutiérrez et al. 2003; Maqueda et al. 2003). These results indicate that another functional role for GABA corelease could be the strengthening of synapses in the developing brain through activation of voltage-gated Ca^{2+} channels by depolarizing GABA (Cherubini et al. 1998). However, under our conditions, coreleased GABA did not activate any $GABA_AR$-mediated response but rather triggered a $GABA_BR$-mediated inhibition of EPSC amplitude by down-regulating the Pr and RRP size.

GABA corelease could act as an autocrine mechanism employed by neurons for inducing continuous adjustments in short-term plasticity responses. In agreement with previous observations (Brenowitz et al. 1998), we observed that the $GABA_BR$-mediated inhibition of glutamatergic autapses can switch synaptic responses from low band-pass to high band-pass filtering, strengthening transmission when autapses are stimulated at high rates. Under this perspective, the $GABA_BR$-mediated reduction of glutamate release by coreleased GABA cannot be simply interpreted as an inhibitory homeostatic brake to excitatory transmission. Rather, the effects of coreleased GABA are dependent on the level of activity of the presynaptic neuron. In neurons that are active at very high rates, an initial inhibition of release ultimately results in an enhancement of synaptic strength by preventing depression and increasing facilitation/potentiation of synaptic transmission.

It is now clear that various synapses have the ability to release multiple SVs in response to a single AP (Tong and Jahr 1994). Multivesicular release is pronounced at high Pr and is dynamically regulated by activity (Wadiche and Jahr 2001; Oertner et al. 2002). The ability to release multiple SVs at individual boutons shifts the quantal release of glutamate from a binary to a graded signal until synaptic transmission becomes saturated. Thanks to the ability to corelease GABA and activate presynaptic $GABA_BR$-mediated inhibition, glutamatergic autapses can work longer under a non-saturated condition (McAllister and Stevens 2000), thus extending the dynamic range of synaptic communication and ultimately increasing their information capacity.

We have shown that glutamatergic autapses coreleasing GABA can dynamically change the Pr and thus decrease depression and enhance facilitation/potentiation of synaptic transmission during periods of intense activity. Short-term plasticity plays a central role in synaptic computation (Abbott and Regehr 2004). By converting patterns of APs into different postsynaptic responses, synapses perform various types of temporal filtering and burst detection operations (Dittman et al. 2000). On a short time-scale, this form of plasticity depends on presynaptic changes in the release properties (Varela et al. 1997) that in turn influence the generation of the postsynaptic response. The temporal pattern of postsynaptic responses results from the extent of synaptic facilitation and depression that both depend on the quantal properties of release, predominantly Pr. We demonstrated that a change in Pr by GABA corelease and activation of presynaptic $GABA_BRs$ affects the filtering characteristics of a given synapse.

Until now, GABA corelease, in the early postnatal life, was interpreted as a source of correlated GABAergic activity playing a crucial role in functional maturation of adult neuronal circuits or a homeostatic mechanism preserving neurons from the

excessive postsynaptic depolarization and the emergence of seizures (Safiulina and Cherubini 2009). Based on these novel findings, GABA corelease also represents an autocrine mechanism that endows excitatory synapses with the ability to actively tune their filtering properties on the basis of the firing frequency to ensure the best output/input ratio and information transfer across the synapse.

Methods

Ethical Approval

All experiments were carried out in accordance with the guidelines established by the European Community Council (Directive 2010/63/EU of 22 September 2010) and were approved by the Italian Ministry of Health. Autaptic hippocampal neurons were prepared from wild-type C57BL6/J mice (Charles River) or from GAD67-GFP transgenic mice (generous gift of Prof Y. Yanagawa; Tamamaki et al. 2003). Heterozygous mice for the GAD67-GFP allele were mated with C57BL/6 wild-type mice to obtain the heterozygous mice whose GABAergic neurons specifically express fluorescence of GFP (Fig. 3). Mice were sacrificed by CO_2 inhalation, and 17- to 18-day embryos (E17–18) were removed immediately by cesarean section.

Hippocampal Autaptic Cultures

Primary cultures of hippocampal neurons were prepared as described before (Baldelli et al. 2005, 2007). In brief, hippocampi were dissociated by enzymatic digestion in 0.125% Trypsin for 20 min at 37 °C and then triturated with a fire-polished Pasteur pipette. No antimitotic drugs were added to prevent glia proliferation. Autaptic neurons were prepared as described previously (Bekkers and Stevens 1991; Chiappalone et al. 2009) with slight modifications. Dissociated neurons were plated at very low density (20 cells/mm^2) on microdots (40–300 μm in diameter) obtained by spraying a mixture of poly-D-lysine (0.1 mg/mL) and collagen (0.25 mg/mL) on Petri dishes or glass coverslip, previously pretreated with 0.15% agarose. Under this culture conditions, each coverslip showed about 10 isolated single autaptic neurons grown on polylysine microdots. Electrophysiological experiments were conducted on single and isolated autaptic neurons between 10 and 15 div.

Primary Antibodies

Antibodies against VGAT (Mouse, 1 : 500, # 131 011; Rabbit, 1 : 500 #131 003), VGLUT1 (Guinea Pig, 1 : 500 # 135 304; Mouse, 1 : 300, # 135 511); GAD67 (Guinea Pig, 1 : 500, # 198 104); $GABA_A\gamma2$ (Rabbit, 1 : 500, # 224 003) and MAP2 (Guinea Pig, 1 : 500, # 188 004) were obtained from Synaptic System. Anti-GABA (Rabbit, 1 : 1000, # A2052) was obtained from Sigma–Aldrich; anti-$GABA_BR1$ (Rabbit, 1 : 250, # sc-14006) was purchased from Santa Cruz; anti Prox1 (Mouse, 1:500, # MAB5652) and anti Calretinin (Rat; 1 : 1000; # AB5054) were obtained from Millipore.

Immunocytochemistry

Cultured autaptic neurons were fixed with 4% paraformaldehyde in 0.1 M phosphate buffer, pH 7.4 for 20 min at room temperature. After several washes in phosphate-buffered saline (PBS), neurons were incubated for 10 min in 50 mM NH_4Cl, permeabilized and blocked for 30 min in 5% normal goat serum (NGS)/0.1% saponin in PBS. Samples were incubated with primary antibodies diluted in 5% NGS/0.1% saponin in PBS up to 2 h. Coverslips were then washed twice in 0.1% saponin in PBS and blocked for 10 min in 5% NGS/0.1% saponin in PBS before being incubated in the same buffer with Alexa-conjugated secondary antibodies (1 : 500, Invitrogen). After several washes in PBS, coverslips were mounted using Prolong Gold antifade reagent with DAPI staining (Invitrogen). As control for the staining and the acquisition procedure, primary antibodies were omitted. Images were acquired using a ×63 objective in a Leica SP5 confocal microscope (Leica Microsystems). Acquired images were analyzed using the ImageJ software (rsb.info.nih.gov/ij/). Only true autaptic neurons (presence of a single DAPI-stained nucleus or DIC image of a single neuron per microisland) were analyzed.

The images of the 3 channels corresponding to VGAT, GABA and VGLUT1 stainings were automatically thresholded, and the values of the mean intensity of the different channels were recorded. Colocalization analysis was performed using the JACoP plug-in of ImageJ Software: for each multichannel acquired image, the colocalization analysis was performed on a manually selected region of interest (ROI) that contained one single autaptic bouton (5 randomly selected autapses were analyzed per autaptic neuron). The Pearson's correlation was performed on single putative excitatory synaptic contacts in which the VGLUT1 signal was detected. Multiple ROIs were defined on the VGLUT1-positive puncta. The other markers GABA, VGAT and $GABA_{A/B}$Rs were thus detected in the same VGLUT1-positive ROIs, and the Pearson's correlations between VGLUT1 and each other marker were computed using a plugin of the ImageJ Software.

Pearson's correlation coefficient was calculated for each autapse as an index of the colocalization of 2 channels (namely, VGLUT1/VGAT, VGLUT1/GABA, VGLUT1/$GABA_A\gamma_2$R or VGLUT1/$GABA_BR_1$).

Patch-Clamp Recordings, Data Acquisition, and Analysis

Whole-cell patch-clamp recordings were made, as previously described (Baldelli et al. 2007; Valente et al. 2011). Patch pipettes, prepared from thin borosilicate glass (Hilgenberg), were pulled and fire-polished to a final resistance of 2–4 MΩ when filled with standard internal solution. Evoked EPSCs were recorded using a double EPC-10 amplifier (HEKA Electronic). For whole-cell recordings, cells were maintained in a standard external solution containing (in mM): 140 NaCl, 2 $CaCl_2$, 1 $MgCl_2$, 4 KCl, 10 glucose, and 10 HEPES (pH 7.3 with NaOH). Unless otherwise indicated, D-(-)-2-amino-5-phosphonopentanoic acid (D-APV; 50 μM; Tocris) and bicuculline methiodide (30 μM, Tocris) were added to the Tyrode external solution to block *N*-methyl-D-aspartate (NMDA) and $GABA_A$Rs, respectively. The standard internal solution contained (in mM): 126 K^+ Gluconate, 4 NaCl, 1 $MgSO_4$, 0.02 $CaCl_2$, 0.1 BAPTA, 15 glucose, 5 HEPES, 3 ATP, and 0.1 GTP (pH 7.2 with KOH). The selective $GABA_B$Rs antagonist ((2S)-3-[[(1S)-1-(3,4-Dichlorophenyl)ethyl]amino-2-hydroxypropyl](phenylmethyl)phosphinic acid hydrochloride; CGP58845 hydrochloride; 5 μM), the selective $GABA_B$Rs agonist, ((R)-4-Amino-3-(4-chlorophenyl)butanoic acid, baclofen 20 μM, Tocris), the group II mGluR receptor blocker ((2S,2′R,3′R)-2-(2′,3′-Dicarboxycyclopropyl)glycine, DCG-IV, 1 μM, Tocris), the GAT-1 inhibitor (1-(4,4-Diphenyl-3-butenyl)-3-piperidinecarboxylic acid hydrochloride, SKF-89976A hydrochloride, 50 μM, Tocris), the peptide blocker for GIRKs (sequence: ALCNCNRIIIPHQCWKKCGKK, tertiapin-Q, 50 nM, Tocris), the A1 receptor blocker (8-ciclopenti-1,3-dipropilxantine, DPCPX; 1 μM, Tocris), and the group II/III mGluR receptor blocker (2-[(1S,2S)-2-carboxycyclopropyl]-3-(9H-xanthen-9-yl)-D-alanine; LY341495, 4 μM, Tocris) were dissolved the same day of the experiments in the external solution. To induce a large loading of GABA into glutamatergic autapses (Bekkers 2005), the external solution containing (in mM): 125 NaCl, 3 KCl, 2

$CaCl_2$, 1 $MgCl_2$, 10 glucose, 25 HEPES, and 25 mannitol (pH 7.4 with NaOH) was switched to a "GABA loading solution" containing (in mM): 40 NaCl, 40 KCl, 2 $CaCl_2$, 1 $MgCl_2$, 10 glucose, 25 HEPES, and 100 GABA (pH 7.4 with NaOH). Under this condition, the standard internal solution contained (in mM): 135 KCl, 7 NaCl, 1 EGTA, 2 $MgCl_2$, 2 Na_2ATP, 0.3 NaGTP, and 10 HEPES, (pH 7.3 with KOH). With the exception of GABA-loading procedure, all the patch-clamp recordings were performed in stop-flow condition. Concentrated (10X) stock solutions of drugs (CGP, bicu, etc.) were diluted 1 : 10 in the extracellular solution to reach the required concentration. The "GABA loading solution" was applied with a gravity-driven local perfusion system at a flow rate of about 200 μL/min, with the outlet located within 100 μm of the patched cell. Neurons were voltage clamped at −70 mV, and APs were evoked by depolarizing the cell body to +40 mV for 0.5 ms at 0.1 Hz. Evoked EPSCs were acquired at 10–20 kHz of sample frequency and filtered at half the acquisition rate with an 8-pole low-pass Bessel filter. Recordings with leak currents of more than 100 pA or series resistance of more than 15 MΩ were discarded. The membrane potentials in our whole-cell recordings were uncorrected for Donnan liquid junction potentials of 9 mV (Neher 1992). All experiments were performed at room temperature (22–24°C). Data acquisition was performed using PatchMaster program (HEKA). Data were analyzed with the FitMaster software version 2.71 (HEKA), Origin 8.6 (OriginLab Corporation; Northampton), and GraphPad Prism 5 (GraphPad Software, Inc.). Evoked EPSCs were inspected visually, and only those that were not contaminated by spontaneous activity were considered. To calculate the peak current during an isolated stimulus or a train of stimuli, we first subtracted an averaged trace containing the stimulus artifact and the AP current, but lacking any discernable synaptic current (i.e., synaptic failures). Such traces were easily identified toward the end of a train of stimuli, when synaptic depression was maximal. These traces were averaged and scaled to the peak Na^+ current contaminating the EPSC. To analyze the PPR, 2 brief depolarizing pulses were applied to autaptic neurons at 50-ms intervals. For each couple of EPSCs, PPR was calculated as the ratio I_2/I_1, where I_1 and I_2 are the amplitudes of the EPSCs evoked by the conditioning and test stimuli, respectively. The amplitude of I_2 was determined as the difference between the I_2 peak and the corresponding value of I_1 calculated by mono-exponential fitting of the eEPSC decay (Jensen et al. 1999). For the evaluation of PTP, autaptic neurons were depolarized with short HFS (1.5 s at 40 Hz). The maximal PTP induced by tetanic stimulation was determined by measuring the maximal amplitude of the EPSCs, usually obtained 10 s after the train, and the time course of PTP was followed with a stimulation frequency to 0.1 Hz. As the inter-spike interval in the train was shorter than the time needed for an EPSC to return to baseline, the amplitude of $(EPSC)_n$ was calculated as the difference between its peak and the residual amplitude of the previous EPSC. The size of the RRP_{syn} and the probability that any given SV in the RRP will be released (Pr) were calculated using the cumulative amplitude analysis, by summing up peak EPSC amplitudes during 40 repetitive stimuli applied at 40 Hz. This analysis assumes that Pr during the train approaches 1.0 and that depression during the steady-state phase is limited by a constant recycling of SVs with an equilibrium between released and recycled SVs (Schneggenburger et al. 1999). The number of data points to include in the linear fitting of the steady-state phase was evaluated by calculating the best linear fit including the maximal number of points starting from the last data point (i.e., from the 40th eEPSC). The cumulative amplitude profiles of the last 15–20 data points were fitted by linear regression and back-extrapolated to time 0. The intercept with the Y-axis gave the RRP_{syn}, and the ratio between the amplitude of the first EPSC (I_1) and RRP_{syn} yielded the Pr. Our estimation of the RRP size was limited to the synchronous release, because its value yielded a better estimation of the Pr induced by isolated stimulation (10 s of time interval; 0.1 Hz; see Fig. 4) that we used to estimate the effect of CGP on the EPSCs. Indeed, during isolated stimulation or at the beginning of the train, the EPSC amplitude mainly depends on the synchronous RRP size, whereas the contribution of the asynchronous pool is negligible, whereas during the train, there is a slow buildup of the asynchronous release that predominates at the end of the train. It is important to recognize that the quantification of RRP with the cumulative amplitude method or other similar methods (i.e., cumulative charge analysis, multiple probability fluctuation analysis, and sucrose stimulation) can be controversial, as each method used to quantify the RRP relies on different assumptions about release (Stevens and Williams 2007). The cumulative amplitude method assumes that the rate of replenishment from the RP to the RRP is constant and that the Pr progressively increases during the train to reach a value of 1. However, even if the full satisfaction of the above-mentioned assumptions cannot be proved, and the estimation of the real size of the total RRP may not be correct, the goal of this analysis was limited to appreciate the relative changes induced by GABA corelease on the RRP_{syn} size, as previously done by others (Thanawala and Regehr 2013).

Statistical Analysis

The statistical analysis is presented in the figure legends. Data are given as means ± SEM for n = sample size. The normal distribution of experimental data was assessed using Kolmogorov–Smirnov's normality test. The F-test was used to compare variance between 2 sample groups. To compare 2 normally distributed sample groups, the Student's unpaired two-tailed t-test was used, with Welch's correction applied in case the variance of the 2 groups was different. To compare 2 sample groups that were not normally distributed, we used Mann–Whitney's nonparametric U-test. To compare more than 2 normally distributed sample groups, we used one- or two-way ANOVA, followed by either the Bonferroni's test. In cases in which data were not normally distributed, one- and two-way ANOVA were substituted with the Kruskal–Wallis's and Friedman's two-way ANOVA tests, respectively, followed by the Dunn's post hoc multiple comparison test. Alpha levels for all tests were 0.5% (95% confidence intervals). Statistical analysis was carried out by using Prism software (GraphPad Software, Inc.).

Hierarchical cluster analysis (HCA) for small sample was performed using the Origin 8.6 software. HCA was applied to the VGLUT1 versus VGAT double-staining results (Fig. 1B, left) to define an objective criterion to roughly quantify the presence of 3 classes of autaptic contacts: 1) expressing only VGLUT1, 2) expressing only VGAT and 3) expressing both VGLUT1 and VGAT. Then, the bi-dimensional relationship between VGLUT1 versus VGAT intensities has been re-represented by a 3D graph, where the variables: x,y,z correspond to VGLUT1, VGAT and VGLUT1*VGAT, respectively (Fig. 1C) to better distinguish the distinct populations of autaptic contacts.

The dendrogram was the most important result of cluster analysis. It lists all samples and indicates at what level of similarity any 2 clusters are joined. In the dendrogram, the bottom row of nodes represents individual observations, and the remaining nodes represent the clusters to which the data belong, with the vertical lines representing the distance (dissimilarity) among clusters. The distance between merged clusters is monotone

increasing with the level of the merger: the height of each node in the plot is proportional to the value of the intergroup dissimilarity between its 2 daughters. The dendrogram was used for determining the cluster number, and the sudden increase in the difference between adjacent steps was used to identify the appropriate number of clusters to consider.

Supplementary Material

Supplementary material can be found at: http://www.cercor.oxfordjournals.org/

Authors' Contribution

P.V., M.O. and A.R. performed experiments and analyzed data; P.V., F.B. and P.B. designed research, planned the experiments, and wrote the paper.

Notes

We thank Dr Silvia Casagrande (University of Genova, Italy) for precious help with cell cultures and Prof Yuchio Yanagawa (Gunma University, Japan) for sharing GAD67-GFP transgenic mice. *Conflict of Interest*: None declared.

Funding

This work was supported by research grants from the Italian Ministry of University and Research (Progetti di Rilevante Interesse Nazionale to F.B.); the Italian Ministry of Health Progetto Giovani (to P.B.); the Compagnia di San Paolo, Torino (to F.B.); and the FET Proactive 7 Project (Grant EU 270483 to F.B.). The support of Telethon-Italy (Grant GGP09066 to P.B.; Grant GGP13033 to F.B.) is also acknowledged.

References

Abbott LF, Regehr WG. 2004. Synaptic computation. Nature. 431: 796–803.

Baldelli P, Fassio A, Valtorta F, Benfenati F. 2007. Lack of synapsin I reduces the readily releasable pool of synaptic vesicles at central inhibitory synapses. J Neurosci. 27:13520–13531.

Baldelli P, Hernandez-Guijo JM, Carabelli V, Carbone E. 2005. Brain-derived neurotrophic factor enhances GABA release probability and nonuniform distribution of N- and P/Q-type channels on release sites of hippocampal inhibitory synapses. J Neurosci. 25:3358–3368.

Bekkers JM. 2005. Presynaptically silent GABA synapses in hippocampus. J Neurosci. 25:4031–4039.

Bekkers JM, Stevens CF. 1991. Excitatory and inhibitory autaptic currents in isolated hippocampal neurons maintained in cell culture. Proc Natl Acad Sci USA. 88:7834–7838.

Beltrán JQ, Gutiérrez R. 2012. Corelease of glutamate and GABA from single, identified mossy fibre giant boutons. J Physiol (Lond). 590:4789–4800.

Bergersen L, Ruiz A, Bjaalie JG, Kullmann DM, Gundersen V. 2003. GABA and GABAA receptors at hippocampal mossy fibre synapses. Eur J Neurosci. 4:931–941.

Brenowitz S, David J, Trussell L. 1998. Enhancement of synaptic efficacy by presynaptic GABA(B) receptors. Neuron. 20:135–141.

Cabezas C, Irinopoulou T, Gauvain G, Poncer JC. 2012. Presynaptic but not postsynaptic GABA signaling at unitary mossy fiber synapses. J Neurosci. 32:11835–11840.

Cesca F, Baldelli P, Valtorta F, Benfenati F. 2010. The synapsins: key actors of synapse function and plasticity. Prog Neurobiol. 91:313–348.

Cherubini E, Martina M, Sciancalepore M, Strata F. 1998. GABA excites immature CA3 pyramidal cells through bicucculline-sensitive and -insensitive chloride-dependent receptors. Perspect Dev Neurobiol. 5:289–304.

Chiappalone M, Casagrande S, Tedesco M, Valtorta F, Baldelli P, Martinoia S, Benfenati F. 2009. Opposite changes in glutamatergic and GABAergic transmission underlie the diffuse hyperexcitability of synapsin i–deficient cortical networks. Cereb Cortex. 19:1422–1439.

Dittman JS, Kreitzer AC, Regehr WG. 2000. Interplay between facilitation, depression, and residual calcium at three presynaptic terminals. J Neurosci. 20:1374–1385.

Dittman JS, Regehr WG. 1996. Contributions of calcium-dependent and calcium-independent mechanisms to presynaptic inhibition at a cerebellar synapse. J Neurosci. 16:1623–1633.

Edwards RH. 2007. The neurotransmitter cycle and quantal size. Neuron. 55:835–858.

Fattorini G, Verderio C, Melone M, Giovedì S, Benfenati F, Matteoli M, Conti F. 2009. VGLUT1 and VGAT are sorted to the same population of synaptic vesicles in subsets of cortical axon terminals. J Neurochem. 110:1538–1546.

Figurov A, Pozzo-Miller LD, Olafsson P, Wang T, Lu B. 1996. Regulation of synaptic responses to high-frequency stimulation and LTP by neurotrophins in the hippocampus. Nature. 381:706–709.

Forgac M. 2007. Vacuolar ATPase: rotary proton pumps in the physiology and pathophysiology. Nat Rev Mol Cell Biol. 8:917–929.

Gaiarsa JL, Tseeb V, Ben-Ari Y. 1995. Postnatal development of pre- and postsynaptic GABAB-mediated inhibitions in the CA3 hippocampal region of the rat. J Neurophysiol. 73: 246–255.

Glykys J, Mody I. 2007. Activation of GABAA receptors: views from outside the synaptic cleft. Neuron. 56:763–770.

Gómez-Lira G, Trillo E, Ramírez M, Asai M, Sitges M, Gutiérrez R. 2002. The expression of GABA in mossy fiber synaptosomes coincides with the seizure-induced expression of GABAergic transmission in the mossy fiber synapse. Exp Neurol. 177: 276–283.

Gottschalk W, Pozzo-Miller LD, Figurov A, Lu B. 1998. Presynaptic modulation of synaptic transmission and plasticity by brain-derived neurotrophic factor in the developing hippocampus. J Neurosci. 18:6830–6839.

Grønborg M, Palvlos NJ, Brunk I, Chua JJ, Münster-Wandowski A, Riedel D, Ahnert-Hilger G, Urlaub H, Jahn R. 2010. Quantitative comparison of glutamatergic and GABAergic synaptic vesicles unveils selectivity for few proteins including MAL2, a novel synaptic vesicles protein. J Neurosci. 30:2–12.

Gutiérrez R. 2009. The dual glutamatergic/GABAergic phenotype of hippocampal granule cells. In: Gutiérrez R, editor. Co-Existence and Co-Release of Classical Neurotransmitters. Mexico City (MX): Springer Science Business Media. p. 181–202.

Gutiérrez R. 2003. The GABAergic phenotype of the "glutamatergic" granule cells of the dentate gyrus. Prog Neurobiol. 71: 337–358.

Gutiérrez R. 2000. Seizures induce simultaneous GABAergic and glutamatergic transmission in the dentate gyrus-CA3 system. J Neurophysiol. 84:3088–3090.

Gutiérrez R, Heinemann U. 2006. Co-existence of GABA and Glu in the hippocampal granule cells: implications for epilepsy. Curr Top Med Chem. 6:975–978.

Gutiérrez R, Heinemann U. 2001. Kindling induces transient fast inhibition in the dentate gyrus-CA3 projection. Eur J Neurosci. 13:1371–1379.

Gutiérrez R, Romo-Parra H, Maqueda J, Vivar C, Ramirez M, Morales MA, Lamas M. 2003. Plasticity of the GABAergic phenotype of the "glutamatergic" granule cells of the rat dentate gyrus. J Neurosci. 23:5594–5598.

Hnasko TS, Edwards RH. 2012. Neurotransmitters corelease: mechanism and physiological role. Annu Rev Physiol. 74: 225–243.

Hökfelt T, Johansson O, Ljungdahl A, Lundberg JM, Schultzberg M. 1980. Peptidergic neurones. Nature. 284:515–521.

Iwano T, Masuda A, Kiyonari H, Enomoto H, Matsuzaki F. 2012. Prox1 postmitotically defines dentate gyrus cells by specifying granule cell identity over CA3 pyramidal cell fate in the hippocampus. Development. 16:3051–3062.

Jensen K, Lambert JD, Jensen MS. 1999. Activity-dependent depression of GABAergic IPSCs in cultured hippocampal neurons. J Neurophysiol. 82:7288–7297.

Jonas P, Bischofberger J, Sandkühler J. 1998. Corelease of two fast neurotransmitters at a central synapse. Science. 281:419–424.

Kamiya H, Shinozaki H, Yamamoto C. 1996. Activation of metabotropic glutamate receptor type 2/3 suppresses transmission at rat hippocampal mossy fibre synapses. J Physiol. 493:447–455.

Kao YH, Lassová L, Bar-Yehuda T, Edwards RH, Sterling P, Vardi N. 2004. Evidence that certain retinal bipolar cells use both glutamate and GABA. J Comp Neurol. 478:207–218.

Kempermann G, Jessberger S, Steiner B, Kronenberg G. 2004. Milestones of neuronal development in the adult hippocampus. Trends Neurosci. 8:447–452.

Li WC, Soffe SR, Roberts A. 2004. Glutamate and acetylcholine corelease at developing synapses. Proc Natl Acad Sci USA. 101:15488–15493.

López-Bendito G, Shigemoto R, Kulik A, Vida I, Fairén A, Luján R. 2004. Distribution of metabotropic GABA receptor subunits GABAB1a/b and GABAB2 in the rat hippocampus during prenatal and postnatal development. Hippocampus. 14:836–848.

Maqueda J, Ramirez M, Lamas M, Gutiérrez R. 2003. Glutamic acid decarboxylase (GAD) 67, but not GAD65, is constitutively expressed during development and transiently overexpressed by activity in the granule cells of the rat. Neurosci Lett. 353:69–71.

McAllister AK, Stevens CF. 2000. Nonsaturation of AMPA and NMDA receptors at hippocampal synapses. Proc Natl Acad Sci USA. 97:6173–6178.

Medrihan L, Cesca F, Raimondi A, Lignani G, Baldelli P, Benfenati F. 2013. Synapsin II desynchronizes neurotransmitter release at inhibitory synapses by interacting with presynaptic calcium channels. Nat Commun. 4:1512–1525.

Moulder KL, Mennerick S. 2005. Reluctant vesicles contribute to the total readily releasable pool in glutamatergic hippocampal neurons. J Neurosci. 25:3842–3850.

Nadler JV. 2003. The recurrent mossy fiber pathway of the epileptic brain. Neurochem Res. 28:1649–1658.

Neher E. 1992. Correction for liquid junction potentials in patch clamp experiments. Methods Enzymol. 207:123–131.

Oertner TG, Sabatini BL, Nimchinsky EA, Svoboda K. 2002. Facilitation at single synapses probed with optical quantal analysis. Nat Neurosci. 5:657–664.

Rao A, Cha EM, Craig AM. 2000. Mismatched appositions of presynaptic and postsynaptic components in isolated hippocampal neurons. J Neurosci. 20:8344–8353.

Romo-Parra H, Vivar C, Maqueda J, Morales MA, Gutiérrez R. 2003. Activity-dependent induction of multitransmitter signaling onto pyramidal cells and interneurons of hippocampal area CA3. J Neurophysiol. 89:3155–3167.

Rost BR, Nicholson P, Ahnert-Hilger G, Rummel A, Rosenmund C, Breustedt J, Schmitz D. 2011. Activation of metabotropic GABA receptors increases the energy barrier for vesicle fusion. J Cell Sci. 124:3066–3073.

Ruiz A, Fabian-Fine R, Scott R, Walker MC, Rusakov DA, Kullmann DM. 2003. $GABA_A$ receptors at hippocampal mossy fibers. Neuron. 39:961–973.

Safiulina VF, Caiati MD, Sivakumaran S, Bisson G, Migliore M, Cherubini E. 2010. Control of GABA Release at Mossy Fiber-CA3 Connections in the Developing Hippocampus. Front Synaptic Neurosci. 2:1–11.

Safiulina VF, Cherubini E. 2009. At immature mossy fibers-CA3 connections, activation of presynaptic $GABA_B$ receptors by endogenously released GABA contributes to synapses silencing. Front Cell Neurosci. 3:1–11.

Safiulina VF, Fattorini G, Conti F, Cherubini E. 2006. GABAergic signaling at mossy fiber synapses in neonatal rat hippocampus. J Neurosci. 26:597–608.

Sakaba T, Neher E. 2003. Direct modulation of synaptic vesicle priming by GABA(B) receptor activation at a glutamatergic synapse. Nature. 424:775–778.

Sandler R, Smith AD. 1991. Coexistence of GABA and glutamate in mossy fiber terminals of the primate hippocampus: an ultrastructural study. J Comp Neurol. 303:177–192.

Schneggenburger R, Meyer AC, Neher E. 1999. Released fraction and total size of a pool of immediately available transmitter quanta at a calyx synapse. Neuron. 23:399–409.

Schwarzer C, Sperk G. 1995. Hippocampal granule cells express glutamic acid decarboxylase-67 after limbic seizures in the rat. Neurosci. 69:705–709.

Semyanov A, Walker MC, Kullmann DM, Silver RA. 2004. Tonically active GABA A receptors: modulating gain and maintaining the tone. Trends Neurosci. 27:262–269.

Sloviter RS, Dichter MA, Rachinsky TL, Dean E, Goodman JH, Sollas AL, Martin DL. 1996. Basal expression and induction of glutamate decarboxylase and GABA in excitatory granule cells of the rat and monkey hippocampal dentate gyrus. J Comp Neurol. 373:593–618.

Sodickson DL, Bean BP. 1996. GABAB receptor-activated inwardly rectifying potassium current in dissociated hippocampal CA3 neurons. J Neurosci. 16:6374–6385.

Stevens CF, Williams JH. 2007. Discharge of the readily releasable pool with action potentials at hippocampal synapses. J Neurophysiol. 98:3221–3229.

Tamamaki N, Yanagawa Y, Tomioka R, Miyazaki J, Obata K, Kaneko T. 2003. Green fluorescent protein expression and colocalization with calretinin, parvalbumin, and somatostatin in the GAD67-GFP knock-in mouse. J Comp Neurol. 467:60–79.

Thanawala MS, Regehr WG. 2013. Presynaptic calcium influx controls neurotransmitter release in part by regulating the effective size of the readily releasable pool. J Neurosci. 33:4625–4633.

Thompson SM, Gähwiler BH. 1992. Comparison of the actions of baclofen at pre- and postsynaptic receptors in the rat hippocampus in vitro. J Physiol (Lond). 451:329–345.

Tong G, Jahr CE. 1994. Multivesicular release from excitatory synapses of cultured hippocampal neurons. Neuron. 12:51–59.

Treviño M, Gutiérrez R. 2005. The GABAergic projection of the dentate gyrus to hippocampal area CA3 of the rat: pre- and postsynaptic actions after seizures. J Physiol (Lond). 567: 939–949.

Treviño M, Vivar C, Gutiérrez R. 2007. Beta/gamma oscillatory activity in the CA3 hippocampal area is depressed by aberrant

GABAergic transmission from the dentate gyrus after seizures. J Neurosci. 27:251–259.

Uchigashima M, Fukaya M, Watanabe M, Kamiya H. 2007. Evidence against GABA release from glutamatergic mossy fiber terminals in the developing hippocampus. J Neurosci. 27: 8088–8100.

Valente P, Casagrande S, Nieus T, Verstegen AM, Valtorta F, Benfenati F, Baldelli P. 2012. Site-specific synapsin I phosphorylation participates in the expression of post-tetanic potentiation and its enhancement by BDNF. J Neurosci. 32:5868–5879.

Valente P, Fernández-Carvajal A, Camprubí-Robles M, Gomis A, Quirce S, Viana F, Fernández-Ballester G, González-Ros JM, Belmonte C, Planells-Cases R, et al. 2011. Membrane-tethered peptides patterned after the TRP domain (TRPducins) selectively inhibit TRPV1 channel activity. FASEB J. 25:1628–1640.

Varela JA, Sen K, Gibson J, Fost J, Abbott LF, Nelson SB. 1997. A quantitative description of short-term plasticity at excitatory synapses in layer 2/3 of rat primary visual cortex. J Neurosci. 17:7926–7940.

Wadiche JI, Jahr CE. 2001. Multivesicular release at climbing fiber-Purkinje cell synapses. Neuron. 32:301–313.

Walker MC, Ruiz A, Kullmann DM. 2001. Monosynaptic GABAergic signaling from dentate to CA3 with a pharmacological and physiological profile typical of mossy fiber synapses. Neuron. 29:703–715.

Wu LG, Saggau P. 1995. $GABA_B$ receptor-mediated presynaptic inhibition in guinea-pig hippocampus is caused by reduction of presynaptic Ca^{2+} influx. J Physiol (Lond). 485:649–657.

Wu Y, Wang W, Díez-Sampedro A, Richerson GB. 2007. Nonvesicular inhibitory neurotransmission via reversal of the GABA transporter GAT-1. Neuron. 56:851–865.

Zander JF, Münster-Wandowski A, Brunk I, Pahner I, Gómez-Lira G, Heinemann U, Gutiérrez R, Laube G, Ahnert-Hilger G. 2010. Synaptic and vesicular coexistence of VGLUT and VGAT in selected excitatory and inhibitory synapses. J Neurosci. 30: 7634–7645.

Zucker RS, Regehr WG. 2002. Short-term synaptic plasticity. Annu Rev Physiol. 64:355–405.